Homogenization using modified Mori-Tanaka and TFA framework for elastoplastic-viscoelastic-viscoplastic composites: Theory and numerical validation.

Mathilde Barral[a,b], George Chatzigeorgiou[a], Fodil Meraghni[a,*], Renan Léon[b]

[a]*Arts et Métiers ParisTech, LEM3-UMR 7239 CNRS, 4 Rue Augustin Fresnel 57078 Metz, France*
[b]*Valeo-GEEDS Mechanical Metier. 76, rue Auguste Perret 94000 CRETEIL, France*

Abstract

This study proposes a micromechanical model based on a modified multi-scale mean field approach that predicts the overall behavior of long fiber reinforced elastoplastic and viscoelastic-viscoplastic composites. The homogenization method adopted is the Mori-Tanaka scheme combined with the Transformation Field Analysis. Moreover, motivated by the distribution of local fields observed in finite element based homogenization analyses, the proposed approach is extended and introduces a special type of coating between the fibers and the matrix. This extension permits to deal with the overestimation of the global stress-strain response using the classical Mori-Tanaka method. Specifically, the coating has the same initial behavior as the matrix, but the inelastic strain fields are amplified compared to those in the matrix during loading. The constitutive equations governing the proposed approach are provided and the numerical implementation, utilizing the "return mapping algorithm" scheme, is explained in detail. The effectiveness of this new method is demonstrated through extensive numerical validation tests, including non-monotonic and non-proportional loading at different strain rates. The reference solution consists of the full field computation using finite element simulations on the studied Representative Volume Element (RVE).

Keywords: Mean field homogenization, Mori-Tanaka, Transformation Field Analysis, coating, viscoelastic-viscoplastic behavior

*Corresponding author.
Email addresses: mathilde.barral@ensam.eu (Mathilde Barral), georges.chatzigeorgiou@ensam.eu (George Chatzigeorgiou), fodil.meraghni@ensam.eu (Fodil Meraghni), renan.leon@valeo.com (Renan Léon)

1. Introduction

Nowadays the automotive and aeronautic industries are strongly driven by their environmental impact. Aiming at reducing the $C0_2$ emissions while meeting the security requirements, the production of lightweight and resistant composite structures is a critical issue for many manufacturers. The high cost of the experimental evaluation of the effective properties of composite structures motivates the development of predictive modeling of such structures in service loading.

Homogenization and micromechanics methods model composite overall behavior from the local properties of the different constituents and their microstructure. Today there is a plethora of micromechanics strategies. The presentation of the existing multi-scale theories is included in various review articles (Kanouté et al., 2009; Pindera et al., 2009; Geers et al., 2010; Charalambakis et al., 2018). Mean field homogenization methods are low computational, semi-analytical, multi-scale approaches, based on the Eshelby's problem (Eshelby, 1957). The most popular among them, the Mori-Tanaka (Mori and Tanaka, 1973; Benveniste, 1987) and the self-consistent (Hill, 1965) schemes, have been first employed for elastic composites. The extension of the homogenization procedure from linear to nonlinear behavior is a complex task in constant evolution. In the literature, many mean field and finite element based homogenization models have been proposed to study composites showing elastoplastic (Mareau et al., 2012; Fritzen et al., 2012; Wu et al., 2013a; Zecevic and Knezevic, 2018; Kotha et al., 2019), transformation induced plastic (Mahnken et al., 2009), elasto-viscoplastic (Paquet et al., 2011; Fournier et al., 2011; Matsuda et al., 2011; Wu et al., 2017; Rao et al., 2019) elasto-viscoplastic coupled with damage (Dondeti et al., 2012), viscoelastic (Rémond, 2005), viscoelastic-viscoplastic (Aboudi, 2005), coupled thermo-mechanical (Chatzigeorgiou et al., 2018; Li et al., 2019) behavior, as well as damage at the interface between the matrix and the fibers (Despringre, 2015).

In mean field homogenization theories, stress and strain fields are considered homogeneous per phase, which allows to use average information of each constituent instead of the local information in each point. Such approach is problematic for nonlinear composites reinforced by stiff inclusions, since the stress and strain fields are actually non-uniform per phase, in particular in the matrix. In this case, the mean field homogenization approaches generally overestimate the global stress-strain

composites responses (Doghri and Ouaar, 2003; Chaboche et al., 2005). To address the excessive stiff predictions, several authors have adopted the so-called isotropization method (Doghri and Ouaar, 2003; Jiang and Shao, 2009; Doghri et al., 2011; Guo et al., 2011; Miled et al., 2013; Czarnota et al., 2015). This technique consists of using the isotropic part of the matrix tangent operator in the homogenization computations, in order to obtain a softer stress-strain response. The disadvantages of such strategies are explained in detail in section 2. Other authors have introduced variational-incremental (Lahellec and Suquet, 2007; Brassart et al., 2012; Boudet et al., 2016) or incremental-secant models (Wu et al., 2013a). These advanced homogenization schemes are based on the introduction of a linear comparison composite (LCC) and the computation of first and second statistical moments. In the general nonlinear case, these frameworks lead to solving a nonlinear problem for identifying the properties of the comparison composite (Lahellec and Suquet, 2007). Bilger et al. (2007) have combined the LCC technique with the composite spheres assemblage method for porous materials. The matrix phase is subdivided in certain concentric layers of spherical type and each layer is described by its own secant modulus.

The mean field method chosen for the current study is the Mori-Tanaka scheme combined with a modified Transformation Field Analysis (TFA). The TFA method, proposed by Dvorak (1992) and Dvorak and Benveniste (1992), is based on the separation between the elastic and the inelastic parts of the macroscopic strain and utilizes the macroscopic elastic tensor. Furthermore, mean field methods can integrate an additional phase representing one or several coating layers between the matrix and the fibers. In the present work, the coating layer is integrated in the proposed mean field method for capturing more accurately the high inelastic strain concentration around the fibers. The latter is generated by the contrast between the fiber and matrix notably in the non linear regimes and can be evidenced numerically by full field homogenization using finite element computations in the corresponding RVE. The developed mean field homogenization combines the Mori-Tanaka scheme and the TFA method and accounts for the coating layer. The inelastic strains in this coating are related to the inelastic strains in the matrix through a specific correction tensor. With this modification, the model can predict accurately the nonlinear overall response of long fiber reinforced elastoplastic and viscoelastic-viscoplastic composites. The structure of the proposed homogenization framework is such that it allows to be utilized, in a simple way, for isotropic or

anisotropic matrix and any choice of elastoplastic or viscoelastic-viscoplastic evolution laws and activation criteria.

The present paper has the following outline. Section 2 discusses the key factors that motivated the formulation of the proposed approach. Section 3 is devoted to the theoretical background of the method, including the evolution of the proper modifications governing the classical Mori-Tanaka scheme to those utilized for the proposed method. The developed numerical procedure aimed at integrating the nonlinear constitutive law of the matrix in the multi-scale model, is presented in section 4. Section 5 describes the identification strategy performed on composites undergoing elastoplasticity and viscoelasticity-viscoplasticity. This section presents also an extensive validation of the model predictions against reference solutions obtained by full field simulations conducted on load/unload and non-proportional loading paths on the RVEs. Finally, it discusses the relevance of the model in comparison between the proposed mean field and the full field homogenizations and raises possible improvements. The following acronyms are used throughout the text: EP for Elasto-Plastic(ity), VE for Visco-Elastic(ity), VP for Visco-Plastic(ity), E-VP for Elasto-Visco-Plastic(ity) and VE-VP for Visco-Elastic(ity)-Visco-Plastic(ity).

2. Proposed approach: Motivation

The various mean field homogenization theories, like for instance the Mori-Tanaka and the self-consistent, are based on the Eshelby problem. In this problem, a single ellipsoidal shape inhomogeneity is embedded into an infinite matrix, which is subjected to uniform strain at far distance. Mori-Tanaka scheme integrates the interactions between fibers and provides a very cost-effective way of predicting the behavior of a large variety of composite types: different inclusion shapes and orientations, different inclusion properties etc... For heterogeneous elastic multi-phase composites, this scheme is accurate for moderate reinforcement volume fractions. In the mean field homogenization theories, the stress and strain fields in each phase are approximated by their phase averages and thus treated as homogeneous. Such approach is problematic for composites with non-linear material constituents. In the case of non-linear matrix behavior (VE/VP/D), stress and strain fields are distributed non-uniformly in the matrix phase. Moreover, mechanical interactions within the phases are treated in a purely elastic way, due to the hypotheses of the Eshelby problem.

For these two reasons, the mean field approach leads to excessive stiff predictions of the overall stress-strain responses in composites consisting of non-linear matrix and stiff inclusions (Doghri and Ouaar, 2003; Chaboche et al., 2005). In order to deal with the stiffness overestimation of the composite, several authors have adopted the so-called isotropization method on EP (Doghri and Ouaar, 2003; Jiang and Shao, 2009; Doghri et al., 2011), E-VP (Czarnota et al., 2015) and VE-VP (Miled et al., 2013) composites. The method consists of extracting the isotropic part from the anisotropic tangent operator of the matrix phase. The use of the isotropized tangent modulus in the computations may reduce the stiff response.

Different strategies of isotropization are available in the literature. Two different strategies have been presented by various authors (Doghri and Ouaar, 2003; Chaboche et al., 2005; Doghri et al., 2010, 2011) for extracting the isotropic part from the anisotropic local stiffness operator: the spectral decomposition and a general projection method. For elasto-plastic composites, Chaboche et al. (2005) approve the usage of the spectral decomposition, whereas Doghri and Ouaar (2003) consider that both strategies provide similar homogenization results.

Some authors utilize the isotropic part of the reference matrix modulus only for the computation of the polarization tensor (Chaboche and Kanoute, 2003; Chaboche et al., 2005; Jiang and Shao, 2009; Sadowski et al., 2017) while others use the isotropized tangent stiffness only for the evaluation of the Eshelby's tensor (Doghri and Ouaar, 2003; Jiang and Shao, 2009; Miled et al., 2013). The efficiency of the isotropization method actually depends on the local plastic flow rule of the local constitutive model (Jiang and Shao, 2009). In order to predict the mechanical response of a two phases composite consisting of an E-VP matrix and spherical inclusions, Czarnota et al. (2015) proposed a Mori-Tanaka scheme combined with the tangent linearization of viscoplastic response and an additive interaction law. They adopted different strategies of isotropization: predictions with isotropization of the Hill tensor, of the polarization tensor and of the Eshelby's tensor. The authors concluded that the isotropization strategies did not provide an improvement of the results accuracy, compared to their initial method. Finally, Miled et al. (2013) proposed a method that can deal with VE-VP constitutive models, generalizing the incrementally affine linearization method proposed by Doghri et al. (2010) for E-VP materials. However, it has been observed that the agreement between the mean field predictions and the reference Finite Elements (FE) results is

less satisfactory for VE-VP than for EP or E-VP matrix materials. According to the authors, this is due to the VE part of the response: isotropization works better on plasticity and viscoplasticity than on viscoelasticity.

The method proposed in this paper is suitable for composites with rate-dependent and rate-independent matrix behavior. The approach is motivated by the observations and the comparisons between full field and mean field homogenization techniques. Performing FE analysis on a unit cell containing elastic fibers and nonlinear matrix, it is observed that a significant part of the inelastic strain (P, VE or VP) is concentrated around the fibers (Fig. 1a). This strain concentration is non-uniform around the fibers. In a mean field approach, local information at each point cannot be recovered. Nevertheless, one can reasonably assume the existence of a *virtual third phase* around the fiber, named coating, having the same properties as those of the matrix, but whose inelastic strain field is amplified compared to that of the matrix (Fig. 1b). This third phase actually "gathers" the information of the nonlinear strain accumulation around the fibers highlighted by FE calculations. To achieve that, the proposed mean field technique requires a proper calibration from full field homogenization results. The characteristics of the identification procedure and the number of required parameters are explained in detail later in the manuscript.

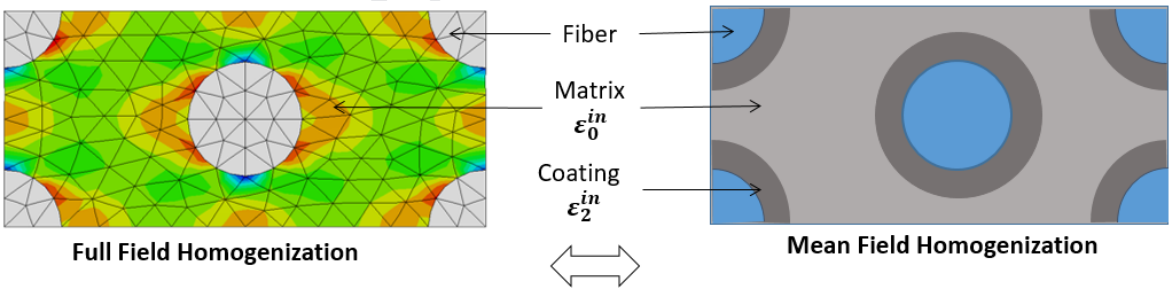

(a) (b)

Figure 1: (a) Inelastic strains generated on a FE unit cell consisting of elastic fibers and inelastic matrix. One can notice the matrix inelastic strains concentrated at the vicinity of the fibers. (b) Adapting a three phase composite model for the mean field homogenization approach captures the evidenced increase of the inelastic strains close to the fibers (coating). It is noted that $\|\boldsymbol{\varepsilon}_2^{in}\| > \|\boldsymbol{\varepsilon}_0^{in}\|$.

The mean field method chosen for this study is the Mori-Tanaka scheme combined with a modified Transformation Field Analysis (TFA). The latter was initially proposed by Dvorak (1992);

Dvorak and Benveniste (1992); Dvorak et al. (1994) and it was extended by other authors (Kattan and Voyiadjis, 1993; Chaboche et al., 2001; Kruch and Chaboche, 2011) to composites with more complex behavior (thermoviscoplasticity, damage...). To resolve the stiff response predictions of the original TFA, Michel and Suquet (2004) have introduced the nonuniform transformation field analysis, where full field calculations take place and the plastic behavior is traced with the help of several plastic modes. An alternative full field TFA implementation has been successfully achieved through the finite volume theory (Cavalcante and Pindera, 2013).

The TFA method is based on the separation of the macroscopic elastic strain $\overline{\boldsymbol{\varepsilon}}$ into an elastic strain $\overline{\boldsymbol{\varepsilon}}^{efl}$ and an inelastic strain $\overline{\boldsymbol{\varepsilon}}^{in}$. The macroscopic stress is given by the expression

$$\overline{\boldsymbol{\sigma}} = \overline{\mathbb{C}} : (\overline{\boldsymbol{\varepsilon}} - \overline{\boldsymbol{\varepsilon}}^{in}), \tag{1}$$

where $\overline{\mathbb{C}}$ denotes the macroscopic elastic modulus. The identification of the macroscopic inelastic strain is based on the concept of eigenstrain fields in a RVE, as explained in detail by Dvorak and Benveniste (1992). The main advantage of the TFA is that the majority of the tensorial operators are derived only once in a preliminary analysis, since they depend only on the per phase elastic moduli, the volume fractions and the geometrical characteristics of the RVE. In the study performed in this article, TFA offers another advantage: the separation of the elastic and the inelastic parts of the total strain allows to work directly on the inelastic strain of the coating, modifying it from that of the matrix (Section 3).

3. Theoretical background

This section presents the main theoretical concepts of the proposed modified Mori-Tanaka TFA scheme, extended to composites with coated fibers.

3.1. Mori-Tanaka scheme

Mori and Tanaka (1973) proposed a method for estimating the average stress in the matrix of a material containing misfitting inclusions with eigenstrains. The method has been further developed, and various authors (Benveniste, 1987; Lagoudas et al., 1991; Desrumaux et al., 2001; Mercier and Molinari, 2009) utilize it to estimate the overall stiffness of a multiphase composite

from given phase moduli, volume fractions, and shapes. It is an efficient analytical mean-field homogenization approach. This theory is formulated using the well-known Eshelby's inhomogeneity problem. Each phase of the composite is treated as homogeneous. The global behavior of the composite is calculated from the average stress and strain fields of each phase. The classical Mori-Tanaka method is briefly discussed here for N-phase composites. The strain $\boldsymbol{\varepsilon}_r$ in the r-th phase is connected with the average macroscopic strain $\overline{\boldsymbol{\varepsilon}}$ through the localization equation

$$\boldsymbol{\varepsilon}_r = \mathbb{A}_r : \overline{\boldsymbol{\varepsilon}}. \tag{2}$$

The strain concentration tensor $\mathbb{A}_r$ is obtained by the relation

$$\mathbb{A}_r = \mathbb{T}_r : \left[\sum_{n=0}^{N} c_n \mathbb{T}_n\right]^{-1}, \tag{3}$$

where c_r denotes the volume fraction of the r-th phase and $\mathbb{T}_r$ is the interaction tensor expressed as

$$\mathbb{T}_r = \left[\mathbb{I} + \mathbb{S}(\mathbb{C}_0) : \mathbb{C}_0^{-1} : [\mathbb{C}_r - \mathbb{C}_0]\right]^{-1}. \tag{4}$$

It is recalled that $\mathbb{I}$ is the fourth order symmetric identity tensor. $\mathbb{S}(\mathbb{C}_0)$ denotes the Eshelby tensor which depends on the properties of the matrix (matrix stiffness tensor $\mathbb{C}_0$), as well as the ellipsoidal geometry of the fiber (form factor). Considering the elastic modulus $\mathbb{C}_r$ of each phase r, as well as the concentration tensors $\mathbb{A}_r$, the overall macroscopic elastic stiffness $\overline{\mathbb{C}}$ is computed as follows:

$$\overline{\mathbb{C}} = \sum_{r=0}^{N} c_r \mathbb{C}_r : \mathbb{A}_r. \tag{5}$$

The last expression is suitable for elastic materials. For inelastic phases, the incremental methods propose to substitute the elastic modulus $\mathbb{C}$ by the tangent modulus $\mathbb{L}^t$. In the TFA, the split of the total strain into an elastic and an inelastic part permits to identify the various concentration tensors only from the local elastic moduli.

3.2. Transformation Field Analysis

For nonlinear analyses, the TFA treats the global behavior of the composites by defining overall constitutive laws that assume the additive decomposition of the total macroscopic strain $\overline{\boldsymbol{\varepsilon}}$ into a

purely elastic fully recoverable strain $\overline{\boldsymbol{\varepsilon}}^{e}$ and an inelastic strain $\overline{\boldsymbol{\varepsilon}}^{in}$, caused by the local inelastic fields

$$\overline{\boldsymbol{\varepsilon}} = \overline{\boldsymbol{\varepsilon}}^{e} + \overline{\boldsymbol{\varepsilon}}^{in}. \tag{6}$$

According to this decomposition, the macroscopic stress $\overline{\boldsymbol{\sigma}}$ is expressed by

$$\overline{\boldsymbol{\sigma}} = \overline{\mathbb{C}} : (\overline{\boldsymbol{\varepsilon}} - \overline{\boldsymbol{\varepsilon}}^{in}). \tag{7}$$

The macroscopic inelastic strain depends on all the microscopic inelastic strains $\boldsymbol{\varepsilon}_r^{in}$

$$\overline{\boldsymbol{\varepsilon}}^{in} \equiv \overline{\boldsymbol{\varepsilon}}^{in}\left(\boldsymbol{\varepsilon}_r^{in}\right). \tag{8}$$

In the original Mori-Tanaka scheme, the strain in the r-th phase $\boldsymbol{\varepsilon}_r$, is expressed by Eq. 2. In the TFA method, this local strain is both a function of the macroscopic strain $\overline{\boldsymbol{\varepsilon}}$ and the local inelastic strains $\boldsymbol{\varepsilon}_r^{in}$

$$\boldsymbol{\varepsilon}_r = \mathbb{A}_r : \overline{\boldsymbol{\varepsilon}} + \sum_{p=0}^{N} \mathbb{A}_{rp}^{in} : \boldsymbol{\varepsilon}_p^{in}. \tag{9}$$

The elastic concentration tensors $\mathbb{A}_r$ remain unchanged (Eq. 3), while the inelastic concentration tensors $\mathbb{A}_r^{in}$ are defined in Dvorak (1992). The latter are computed using the elastic moduli of all phases, their geometrical characteristics and their volume fractions. Actually, the formulation of the inelastic tensor is form-similar to that of the elastic concentration tensors.

The original Eshelby's inhomogeneity problem does not account for coating. Therefore, the classical Mori-Tanaka TFA scheme is revisited in order to address the presence of a nonlinear coating layer between the fiber and the matrix.

3.3. Mori-Tanaka and TFA framework accounting for the coating

The discussed method is based on an extension of the Eshelby's inhomogeneity problem accounting for eigenstrains. The micromechanical approach is modified to study the nonlinear behavior of general ellipsoidal coated fiber reinforced composites with eigenstrains (Berbenni and Cherkaoui, 2010). The equations presented in this subsection are taken from Chatzigeorgiou and Meraghni (2019). The effective composite behavior is obtained by homogenization of the averaged fields studied individually in each phase of a Representative Volume Element (RVE). As it can be

seen in Fig. 2, for unidirectional coated fibers inside a matrix, the RVE is actually modeled by three distinct phases: the matrix (subscript 0), the fibers (subscript 1) and the coatings (subscript 2). The ratio between the volume of the fiber V_1 and the coated fiber $V_1 + V_2$ is denoted as ϕ

$$\phi = \frac{V_1}{V_1 + V_2}. \tag{10}$$

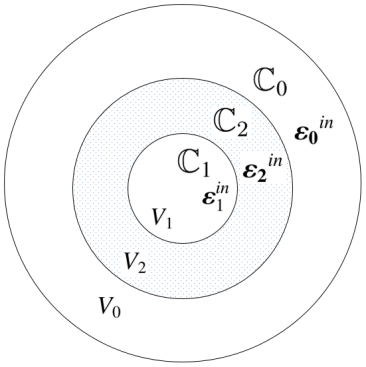

Figure 2: Coated infinitely long cylindrical fiber with homothetic topology inside a matrix. The matrix and the coating layer have uniform eigenstrains $\boldsymbol{\varepsilon_0}^{in}$ and $\boldsymbol{\varepsilon_2}^{in}$ respectively.

Using Eq. 9, the strain $\boldsymbol{\varepsilon}_r$ in the r-th phase for single layer coated fiber composites is defined as

$$\boldsymbol{\varepsilon}_r = \mathbb{A}_r : \overline{\boldsymbol{\varepsilon}} + \mathbb{A}_{r0}^{in} : \boldsymbol{\varepsilon}_0^{in} + \mathbb{A}_{r1}^{in} : \boldsymbol{\varepsilon}_1^{in} + \mathbb{A}_{r2}^{in} : \boldsymbol{\varepsilon}_2^{in}, \qquad r = 0, 1, 2. \tag{11}$$

The elastic concentration tensors $\mathbb{A}_r$ are given by

$$\mathbb{A}_0 = [c_0\mathbb{T}_0 + c_1\mathbb{T}_1 + c_2\mathbb{T}_2]^{-1}, \quad \mathbb{A}_1 = \mathbb{T}_1 : \mathbb{A}_0, \quad \mathbb{A}_2 = \mathbb{T}_2 : \mathbb{A}_0, \tag{12}$$

and the inelastic concentration tensors $\mathbb{A}_{rp}^{in}$ ($r = 0, 1, 2$ and $p = 0, 1, 2$) are obtained by

$$\begin{aligned}
&\mathbb{A}_{00}^{in} = -\mathbb{A}_0 : \left[c_1\mathbb{T}_{10}^{in} + c_2\mathbb{T}_{20}^{in}\right], \quad \mathbb{A}_{01}^{in} = -\mathbb{A}_0 : \left[c_1\mathbb{T}_{11}^{in} + c_2\mathbb{T}_{21}^{in}\right], \quad \mathbb{A}_{02}^{in} = -\mathbb{A}_0 : \left[c_1\mathbb{T}_{12}^{in} + c_2\mathbb{T}_{22}^{in}\right], \\
&\mathbb{A}_{10}^{in} = \mathbb{T}_1 : \mathbb{A}_{00}^{in} + \mathbb{T}_{10}^{in}, \qquad \mathbb{A}_{11}^{in} = \mathbb{T}_1 : \mathbb{A}_{01}^{in} + \mathbb{T}_{11}^{in}, \qquad \mathbb{A}_{12}^{in} = \mathbb{T}_1 : \mathbb{A}_{02}^{in} + \mathbb{T}_{12}^{in}, \\
&\mathbb{A}_{20}^{in} = \mathbb{T}_2 : \mathbb{A}_{00}^{in} + \mathbb{T}_{20}^{in}, \qquad \mathbb{A}_{21}^{in} = \mathbb{T}_2 : \mathbb{A}_{01}^{in} + \mathbb{T}_{21}^{in}, \qquad \mathbb{A}_{22}^{in} = \mathbb{T}_2 : \mathbb{A}_{02}^{in} + \mathbb{T}_{22}^{in}.
\end{aligned} \tag{13}$$

The elastic interaction tensors $\mathbb{T}_r$ are given by the formulas

$$\mathbb{T}_0 = \mathbb{I}, \qquad \mathbb{T}_1 = \left[\phi\mathbb{N}_{10} + [1-\phi]\,\mathbb{N}_{20} : \mathbb{N}_{12}\right]^{-1}, \qquad \mathbb{T}_2 = \mathbb{N}_{12} : \mathbb{T}_1, \tag{14}$$

while the inelastic interaction tensors $\mathbb{T}^{in}_{rp}$ are given by

$$\mathbb{T}^{in}_{10} = -\mathbb{T}_1 : \mathbb{P}_0 : \mathbb{C}_0, \quad \mathbb{T}^{in}_{11} = \mathbb{T}_1 : \left[\phi\mathbb{P}_0 + \left[1-\phi\right]\mathbb{N}_{20} : \mathbb{P}_2\right] : \mathbb{C}_1,$$
$$\mathbb{T}^{in}_{12} = \left[1-\phi\right]\mathbb{T}_1 : \left[\mathbb{P}_0 - \mathbb{N}_{20} : \mathbb{P}_2\right] : \mathbb{C}_2, \qquad \mathbb{T}^{in}_{20} = \mathbb{N}_{12} : \mathbb{T}^{in}_{10},$$
$$\mathbb{T}^{in}_{21} = \mathbb{N}_{12} : \mathbb{T}^{in}_{11} - \mathbb{P}_2 : \mathbb{C}_1, \qquad \mathbb{T}^{in}_{22} = \mathbb{N}_{12} : \mathbb{T}^{in}_{12} + \mathbb{P}_2 : \mathbb{C}_2, \tag{15}$$

where

$$\mathbb{N}_{10} = \mathbb{I} + \mathbb{P}_0 : \left[\mathbb{C}_1 - \mathbb{C}_0\right], \quad \mathbb{N}_{20} = \mathbb{I} + \mathbb{P}_0 : \left[\mathbb{C}_2 - \mathbb{C}_0\right],$$
$$\mathbb{N}_{12} = \mathbb{I} + \mathbb{P}_2 : \left[\mathbb{C}_1 - \mathbb{C}_2\right]. \tag{16}$$

Moreover

$$\mathbb{P}_0 = \mathbb{S}(\mathbb{C}_0) : \mathbb{C}_0^{-1}, \quad \mathbb{P}_2 = \mathbb{S}(\mathbb{C}_2) : \mathbb{C}_2^{-1}. \tag{17}$$

are the symmetric Hill polarization tensors. $\mathbb{S}(\mathbb{C}_2)$ denotes the Eshelby tensor that depends on the coating layer elasticity tensor and the shape of the fibers. The above expressions correspond to homothetic coated fiber composites.

The additional coating layer utilized in this work is fictitious and allows to account for the inelastic strain concentration around the fibers. In the sequel, the way to achieve this goal is explained.

3.4. Mori-Tanaka and TFA framework accounting for the virtual coating

In this subsection, the case is the same as the previous one with the exception that the matrix and the coating have the same elastic modulus (Fig.3).

$$\mathbb{C}_0 = \mathbb{C}_2. \tag{18}$$

Indeed, the matrix and the coating are modeled by the same nonlinear constitutive law. However, the average inelastic strain in the coating $\boldsymbol{\varepsilon}^{in}_2$ is different from that of the matrix $\boldsymbol{\varepsilon}^{in}_0$. As mentioned in section 2, this modification is going to account for the non-uniform strain concentration around the fibers, observed in FE homogenization analysis. A significant part of the inelastic strain of the

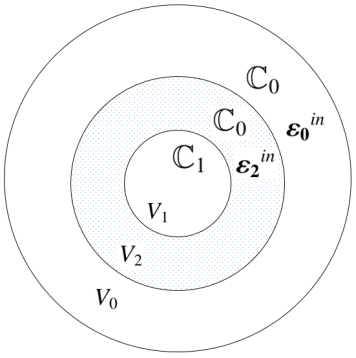

Figure 3: Coated infinitely long cylindrical fiber with homothetic topology inside a matrix. The matrix and the coating layer have uniform eigenstrains $\boldsymbol{\varepsilon_0}^{in}$ and $\boldsymbol{\varepsilon_2}^{in}$ respectively, and same properties.

matrix is concentrated in the virtual coating. The difference between $\boldsymbol{\varepsilon}_2^{in}$ and $\boldsymbol{\varepsilon}_0^{in}$ is then expressed with the help of a correction tensor $\mathbb{Y}$, as follows:

$$\boldsymbol{\varepsilon_2}^{in} = \mathbb{Y} : \boldsymbol{\varepsilon_0}^{in}. \tag{19}$$

The goal of this correction tensor is to assure that the total inelastic strain in the matrix and the coating can provide the correct macroscopic behavior.

For long fiber composites with isotropic constituents, the proposed method requires 4 parameters. The first one is the ratio ϕ which depends on the fiber and the coating volume fractions (Eq. 10). Since the coating is a virtual phase, the choice of ϕ is somehow arbitrary and some criteria are required to limit its range, as explained more precisely in subsection 5.3. The other three parameters are the components of the correction tensor: (γ^N, γ^{ST}, γ^{SL}) (Eq. 20). The correction tensor $\mathbb{Y}$ for composites with infinitely long fibers parallel to the third direction has the following form:

$$\mathbb{Y} = \begin{bmatrix} \gamma^N & 0 & 0 & 0 & 0 & 0 \\ 0 & \gamma^N & 0 & 0 & 0 & 0 \\ 0 & 0 & 1 & 0 & 0 & 0 \\ 0 & 0 & 0 & \gamma^{ST} & 0 & 0 \\ 0 & 0 & 0 & 0 & \gamma^{SL} & 0 \\ 0 & 0 & 0 & 0 & 0 & \gamma^{SL} \end{bmatrix} \tag{20}$$

Note that $\mathbb{Y}(3,3)$ is assumed equal to one, since for applied loading in the longitudinal direction of the fibers classical mean field homogenization without coating and full field homogenization give very close results. In addition, for long stiff elastic fibers, such loading provides an almost elastic response for moderate and high fiber volume fractions.

The computation of the interaction tensors is the first step to evaluate the macroscopic behavior of composite materials through the mean field homogenization approach. As mentioned before, the matrix and the coating have the same elastic moduli. Thus, substituting Eq. 18 in Eq. 14 and Eq. 15 yields to the elastic interaction tensors $\mathbb{T}_r$ and the inelastic interaction tensors $\mathbb{T}^{in}_{rp}$

$$\mathbb{T}_0 = \mathbb{T}_2 = \mathbb{I}, \qquad \mathbb{T}_1 = [\mathbb{I} + \mathbb{S}(\mathbb{C}_0) : \mathbb{C}_0^{-1} : (\mathbb{C}_1 - \mathbb{C}_0)]^{-1}, \tag{21}$$

$$\begin{aligned} &\mathbb{T}^{in}_{10} = -\mathbb{T}_1 : \mathbb{S}(\mathbb{C}_0), \quad \mathbb{T}^{in}_{11} = \mathbb{T}_1 : \mathbb{S}(\mathbb{C}_0) : \mathbb{C}_0^{-1} : \mathbb{C}_1, \quad \mathbb{T}^{in}_{12} = 0, \\ &\mathbb{T}^{in}_{20} = -\mathbb{S}(\mathbb{C}_0), \qquad \mathbb{T}^{in}_{21} = 0, \qquad \mathbb{T}^{in}_{22} = \mathbb{S}(\mathbb{C}_0). \end{aligned} \tag{22}$$

Using the last two expressions and Eq. 19, the elastic $\mathbb{A}_r$ and inelastic $\mathbb{A}^{in}_{rp}$ concentration tensors are written in the following form:

$$\mathbb{A}_0 = \mathbb{A}_2 = [(c_0 + c_2)\mathbb{I} + c_1\mathbb{T}_1]^{-1} \qquad \mathbb{A}_1 = \mathbb{T}_1 : \mathbb{A}_0, \tag{23}$$

$$\begin{aligned} \mathbb{A}^{in}_{00} &= \mathbb{A}_0 : [c_1\mathbb{T}_1 + c_2\mathbb{I}] : \mathbb{S}(\mathbb{C}_0), & \mathbb{A}^{in}_{01} &= -c_1\mathbb{A}_0 : \mathbb{T}_1 : \mathbb{P}_0 : \mathbb{C}_1, \\ \mathbb{A}^{in}_{02} &= -c_2\mathbb{A}_0 : \mathbb{S}(\mathbb{C}_0), & \mathbb{A}^{in}_{10} &= \mathbb{T}_1 : [\mathbb{A}_0 : [c_1\mathbb{T}_1 + c_2\mathbb{I}] - \mathbb{I}] : \mathbb{S}(\mathbb{C}_0), \\ \mathbb{A}^{in}_{11} &= \mathbb{T}_1 : [-c_1\mathbb{A}_0 : \mathbb{T}_1 + \mathbb{I}] : \mathbb{P}_0 : \mathbb{C}_1, & \mathbb{A}^{in}_{12} &= -c_2\mathbb{T}_1 : \mathbb{A}_0 : \mathbb{S}(\mathbb{C}_0), \\ \mathbb{A}^{in}_{20} &= [\mathbb{T}_2 : \mathbb{A}_0 : [c_1\mathbb{T}_1 + c_2\mathbb{I}] - \mathbb{I}] : \mathbb{S}(\mathbb{C}_0), & \mathbb{A}^{in}_{21} &= -c_1\mathbb{T}_2 : \mathbb{A}_0 : \mathbb{T}_1 : \mathbb{P}_0 : \mathbb{C}_1, \\ \mathbb{A}^{in}_{22} &= [-c_2\mathbb{T}_2 : \mathbb{A}_0 + \mathbb{I}] : \mathbb{S}(\mathbb{C}_0). \end{aligned} \tag{24}$$

It is noticed that the TFA technique allows calculating all concentration tensors only once, in a preliminary analysis. As a matter of fact, these tensors depend only on the elastic stiffness tensors, and the shape and volume fraction of the phases, which do not depend on the inelastic fields.

The total strain in the different phases are derived from Eq. 11.

$$\boldsymbol{\varepsilon_0} = \mathbb{A}_0 : \overline{\boldsymbol{\varepsilon}} + \mathbb{A}_0 : [c_1\mathbb{T}_1 : \mathbb{S}(\mathbb{C}_0) + c_2\mathbb{S}(\mathbb{C}_0) : (\mathbb{I} - \mathbb{Y})] : \boldsymbol{\varepsilon_0}^{in}, \tag{25}$$

$$\boldsymbol{\varepsilon_1} = \mathbb{T}_1 : \boldsymbol{\varepsilon_0} - \mathbb{T}_1 : \mathbb{S}(\mathbb{C}_0) : \boldsymbol{\varepsilon_0}^{in}, \tag{26}$$

$$\boldsymbol{\varepsilon_2} = \boldsymbol{\varepsilon_0} - \mathbb{S}(\mathbb{C}_0) : (\mathbb{I} - \mathbb{Y}) : \boldsymbol{\varepsilon_0}^{in}, \tag{27}$$

where it has been taking into account that the inelastic strains in the fibers are null ($\boldsymbol{\varepsilon_1} = 0$).

The stress and the inelastic strain in the matrix are obtained from the corresponding constitutive law, through an iterative procedure that is explained later in the manuscript. The stress in the coating $\boldsymbol{\sigma_2}$ is evaluated from the expression

$$\boldsymbol{\sigma_2} = \mathbb{C}_0 : (\boldsymbol{\varepsilon_2} - \boldsymbol{\varepsilon_2}^{in}). \tag{28}$$

Substituting Eq. 19 and Eq. 27 in Eq. 28, one can easily show that

$$\begin{aligned} \boldsymbol{\sigma_2} &= \mathbb{C}_0 : \left[\boldsymbol{\varepsilon_0} - \boldsymbol{\varepsilon_0}^{in}\right] + \mathbb{C}_0 : [\mathbb{I} - \mathbb{S}(\mathbb{C}_0) + \mathbb{S}(\mathbb{C}_0) : \mathbb{Y} - \mathbb{Y}] : \boldsymbol{\varepsilon_0}^{in} \\ &= \boldsymbol{\sigma_0} + \mathbb{C}_0 : [\mathbb{I} - \mathbb{S}(\mathbb{C}_0)] : [\mathbb{I} - \mathbb{Y}] : \boldsymbol{\varepsilon_0}^{in}. \end{aligned} \tag{29}$$

The stress in the coating is subdivided into two terms. The first one describes the constraint far away in the matrix ($\boldsymbol{\sigma_0}$). The second term represents the overstress in the vicinity of the fiber generated by the high concentration of the inelastic strain around the fiber.

Finally, the overall macroscopic stress is calculated as follows:

$$\overline{\boldsymbol{\sigma}} = c_0\boldsymbol{\sigma_0} + c_1\boldsymbol{\sigma_1} + c_2\boldsymbol{\sigma_2}. \tag{30}$$

It should be noted that the Eshelby tensor $\mathbb{S}(\mathbb{C}_0)$, in the general case, can be evaluated numerically using the methodology proposed by Gavazzi and Lagoudas (1990). For composites consisting of an isotropic matrix and infinitely long cylindrical fibers, an analytic expression of the Eshelby tensor exists in the literature (Mura, 1987).

4. Numerical implementation

Finite Element (FE) methods are widely used to solve systems of equations that are strongly nonlinear. Therefore, a numerical procedure is established to implement the presented nonlinear constitutive model through a FORTRAN User MATerial (UMAT) subroutine linked with Abaqus software. Abaqus is a versatile FE computing package that allows the user to define its own material constitutive law with custom subroutines. In this section, the adopted computational algorithm and the return mapping algorithm are described, followed by the tangent modulus algorithm.

4.1. Computational algorithm

The computational algorithm in ABAQUS/Standard is illustrated in Fig. 4 through a flowchart for nonlinear composites. The main idea of the numerical time discretization algorithm is that, at the time interval $[t_n, t_{n+1}]$, the FE solver transfers to the return mapping algorithm: a) the increment of total strain $\Delta\overline{\boldsymbol{\varepsilon}}^{(n+1)}$, b) the macro strain $\overline{\boldsymbol{\varepsilon}}^{(n)}$, c) all history variables (or internal variables) $\overline{\boldsymbol{\mathcal{V}}}^{(n)}$, and d) the macro stress $\overline{\boldsymbol{\sigma}}^{(n)}$. Inversely, the return mapping algorithm provides to the FE solver: a) the effective stress $\overline{\boldsymbol{\sigma}}^{(n+1)}$ and the internal variables $\overline{\boldsymbol{\mathcal{V}}}^{(n+1)}$ through a constitutive law algorithm, and b) the effective tangent modulus $\overline{\mathbb{L}}^{t(n+1)}$ through a tangent modulus algorithm. It is noted that the internal variables $\overline{\boldsymbol{\mathcal{V}}}^{(n)}$ include the local strains $\boldsymbol{\varepsilon}_r^{(n)}$, the local stresses $\boldsymbol{\sigma}_r^{(n)}$ and the local internal variables $\boldsymbol{\mathcal{V}}_r^{(n)}$ of each phase r.

4.2. Return mapping algorithm

Based on a backward Euler time implicit numerical scheme, the value of a given quantity x is updated from the previous time increment n to the current n+1 such as $x^{(n+1)} = x^{(n)} + \Delta x^{(n+1)}$. Such an implicit relation is usually solved iteratively, using the Newton Raphson method (Simo and Hughes, 1998). The current value is updated for each constitutive law correction iteration k by: $x^{(n+1)(k+1)} = x^{(n+1)(k)} + \delta x^{(n+1)(k)}$ until $x^{(n+1)}$ converges. Therefore, the local strain in the r-th phase presented in Eq. 9 can take the form

$$\boldsymbol{\varepsilon}_r^{(n+1)(k)} = \mathbb{A}_r : (\overline{\boldsymbol{\varepsilon}}^{(n)} + \Delta\overline{\boldsymbol{\varepsilon}}^{(n+1)}) + \sum_{r=0}^{N} \mathbb{A}_{rp}^{in} : \boldsymbol{\varepsilon}_p^{in(n+1)(k)}, \tag{31}$$

considering that

$$\boldsymbol{\varepsilon}_r^{in(n+1)(0)} = \boldsymbol{\varepsilon}_r^{in(n)}. \tag{32}$$

The local strain $\boldsymbol{\varepsilon}_r^{(n+1)(k)}$ is given as an input variable to the local constitutive law of the considered phase, in order to compute the local stress $\boldsymbol{\sigma}_r^{(n+1)(k+1)}$, the local tangent modulus $\mathbb{L}_r^{(n+1)(k+1)}$ (utilized thereafter in the tangent modulus algorithm) and the local inelastic strain $\boldsymbol{\varepsilon}_r^{in(n+1)(k+1)}$. The latter is assigned to the local internal variables $\boldsymbol{\mathcal{V}}_r^{(n+1)(k+1)}$. It is noticed that the stress in the coating is computed from Eq. 29 which expresses the coating stress from the matrix one. As a matter of fact, the coating being only a virtual phase, does not have its own constitutive law. In order to have a micromechanical consistency, the local strain $\boldsymbol{\varepsilon}_r^{(n+1)(k)}$ is checked at each correction iteration k

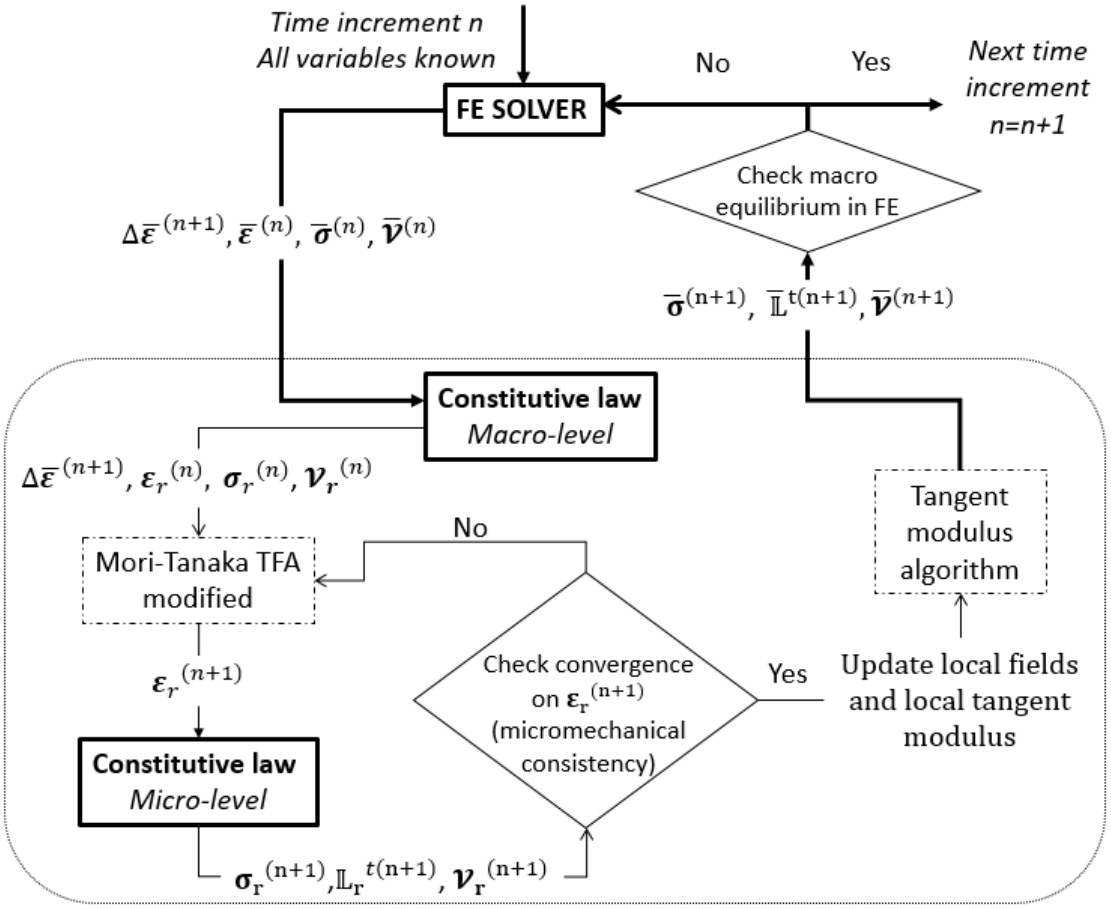

Figure 4: Flowchart of the computational algorithm in ABAQUS/Standard, for the nonlinear response of composites. Additional correction loops at each correction iteration and for each nonlinear phase r are required until reaching local convergence.

and for each nonlinear phase r until reaching local convergence. Specifically, additional correction loops are required until all the local strains remain constant, before updating the other local variables, as shown in Fig. 4.

4.3. Tangent calculations

The global finite element solver requires, in addition to the macroscopic stress, the effective tangent operator $\overline{\mathbb{L}}^{t}$ of the composite. Three possible choices for the tangent operator can be adopted: 1) The use of the elastic modulus. This choice is too stiff compared to the real tangent modulus and requires excessive reduction of the time step, as well as several iterations to reach the global convergence. 2) The real tangent modulus. Its computation is problematic for this model,

since it depends on the local tangent modulus of the coating. The latter is a virtual phase having a fictitious tangent modulus, which is difficult to evaluate properly. In addition, the coating is subjected to important inelastic strains which produce too soft response. Therefore, a fictitious tangent modulus for the coating may cause numerical instabilities. 3) A compromise combining the two previous cases and using an intermediate tangent operator between the elastic and the real tangent modulus.

In this study, an important simplification has been assumed: the tangent moduli of the coating and the matrix are considered the same

$$\mathbb{L}_2^t = \mathbb{L}_0^t. \tag{33}$$

The $\mathbb{L}_0^t$ is computed for the inelastic strain of the matrix and the matrix/coating system is treated as a matrix phase, whose volume fraction is denoted $\tilde{c}_0$

$$c_0 + c_2 \rightarrow \tilde{c}_0. \tag{34}$$

It is important to emphasize that these simplifications are considered only for the computation of the macroscopic tangent modulus. These assumptions allow to obtain a macroscopic tangent modulus which gives an effective global convergence in the FE analysis. Even though the proposed tangent operator deviates from the real tangent, its use does not affect the results and the obtained macroscopic response is still accurate. Nevertheless, the computation of a more accurate tangent operator remains an open topic for further research.

The numerical estimation of the macroscopic tangent modulus requires first the evaluation of the tangent interaction tensor of the fibers $\mathbb{T}_1^t$. However, the latter is different from the elastic one given in Eq. 21, since it depends on the anisotropic tangent modulus of the matrix $\mathbb{L}_0^t$

$$\mathbb{T}_1^t = [\mathbb{I} + \mathbb{S}^t(\mathbb{L}_0^t) : \mathbb{L}_0^{t\,-1} : (\mathbb{C}_1 - \mathbb{L}_0^t)]^{-1}, \tag{35}$$

where $\mathbb{S}^t(\mathbb{L}_0^t)$ denotes the tangent Eshelby tensor that depends on the anisotropic tangent modulus of the matrix $\mathbb{L}_0^t$. Therefore, the tangent Eshelby tensor has to be numerically evaluated using the methodology proposed by Gavazzi and Lagoudas (1990).

The tangent localization tensors in the matrix $\mathbb{A}_0^t$ and in the fibers $\mathbb{A}_1^t$ are given by the expres-

sions

$$\mathbb{A}_0^t = [\tilde{c}_0\mathbb{I} + c_1\mathbb{T}_1^t]^{-1}, \qquad \mathbb{A}_1^t = \mathbb{T}_1^t : \mathbb{A}_0^t. \tag{36}$$

Finally, given the actual tangent moduli $\mathbb{L}_r^t$, as well as the tangent concentration tensors $\mathbb{A}_r^t$, the macroscopic tangent operator $\overline{\mathbb{L}}^t$ takes the form

$$\overline{\mathbb{L}}^t = \tilde{c}_0\mathbb{L}_0^t : \mathbb{A}_0^t + c_1\mathbb{C}_1 : \mathbb{A}_1^t. \tag{37}$$

5. Identification strategy and validation

In this section, the previously formulated constitutive model is applied to describe the behavior of composites consisting of a matrix showing EP or VE-VP behavior and long elastic glass fibers. The modified Mori-Tanaka TFA method leads to a low number of parameters with a certain simplicity regarding their identification. This section focuses on the identification strategy of the model parameters and their validation, by comparing the predictions of the model against data obtained from FE simulations on loaded and unloaded EP composites. Finally, to provide a better understanding of the model, the latter's capabilities to capture the anisotropic response of nonlinear composites are demonstrated through non-proportional multi-axial simulations performed and analyzed on EP and VE-VP composites. The input parameters for the constitutive law are the matrix parameters presented in the sequel, the fiber properties, the fiber volume fraction (c_1), the ratio ϕ (Eq. 10) and the three parameters related to the correction tensor $\mathbb{Y}$ (γ^N, γ^{ST}, γ^{SL}). In the proposed methodology, the $\mathbb{Y}$ tensor is assumed constant (invariant of the loading path and the strain level). For the studied numerical examples this hypothesis is shown to be acceptable. However, in case of other types of matrix constitutive laws, in which the evolution of plasticity is strongly nonuniform, it is possible that the $\mathbb{Y}$ tensor becomes non constant and dependent on the equivalent stress level.

5.1. 3D FE representative unit cell for the parameters identification

The identification and validation of the model are performed from FE analyses data on a 3D unit cell of a two-phase composite with periodic microstructure, illustrated in Fig. 5. The size of the unit cell is 1.316 x 1 x 0.76 and its volume is 1, considering hexagonal symmetry in the

microstructure. The long fibers volume fraction ranges from 10% to 50%. The mesh consists of approximately 8000 ten-node tetrahedral elements (C3D10 in ABAQUS) for all the volume fractions.

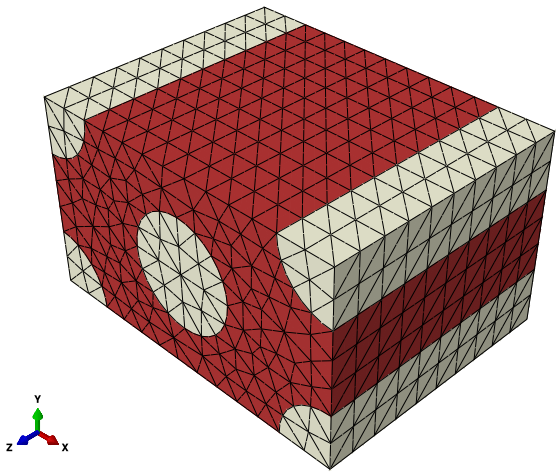

Figure 5: 3D meshed unit cell of a two phase composite: a non-linear matrix and infinitely long cylindrical fibers oriented in the z direction.

5.2. *Choice of matrix material*

In the case of the EP matrix, the material parameters are those utilized in the example of Chaboche and Kanoute (2003). For the VE-VP matrix, the parameters are representing the behavior of a polymer. The choice of these materials serves to illustrate the need for the modification of the micromechanics approach, since the predictions derived from the classical Mori-Tanaka TFA method are very rigid and quite different from the FE reference results.

5.2.1. *Composites with elastoplasic matrix*

The rate-independent behavior of the first composite is simulated on a wide range of fiber volume fractions ranging from 10% to 50%. The elastoplastic matrix, with Young's modulus $E = 75$ GPa and Poisson's ratio $\nu = 0.3$, follows an isotropic hardening power law

$$eq(\boldsymbol{\sigma}) = R_0 + Hp^{\alpha}, \tag{38}$$

with $R_0 = 75$ MPa, $H = 416$ MPa and $\alpha = 0.3895$, where $eq(\boldsymbol{\sigma})$ and p are the Von Mises equivalent stress and the cumulative plastic strain respectively. The fibers are elastic with Young's modulus $E = 400$ GPa and Poisson's ratio $\nu = 0.2$.

5.2.2. Composites with viscoelastic-viscoplastic matrix

The second composite consists of a rate-dependent matrix reinforced by 20% volume fraction of fibers. The fibers are elastic with Young's modulus $E = 72.4$ GPa and Poisson's ratio $\nu = 0.22$. The constitutive law of the matrix material is defined through a phenomenological model for viscoelasticity and viscoplasticity in semi-crystalline polymers. This constitutive law is based on the formulation of Praud et al. (2017), under the small strain assumption, and isothermal conditions. The rheological model consists of N viscoelastic Kelvin Voigt branches and a viscoplastic branch. In this study, two viscoelastic Kelvin Voigt branches are utilized in order to capture a sufficiently wide range of strain rates while keeping a reasonable computing time. The rheological parameters are collected in table 1, where

Table 1: Constitutive model parameters for the VE-VP matrix phase. For the sake of simplicity, the subscript 0 indicated for the matrix phase is removed since this section is totally devoted to the matrix.

Viscoelasticity		**Viscoplasticity**	
Parameter	**Value**	**Parameter**	**Value**
E_e	2760 MPa	R_0	30 MPa
E_{v_1}	5500 MPa	K	250 MPa
η_{v_1}	2160 MPa.s	n	0.4
E_{v_2}	7540 MPa	H	60 MPa.s^m
η_{v_2}	168140 MPa.s	m	0.3

- E_e and E_{v_i} are the Young's modulus and the viscous modulus of the i^{th} viscoelastic branch respectively,
- η_{v_i} are the viscous coefficients,

- R_0 is the yield stress,
- K and n are the hardening modulus and the hardening exponent respectively, and they are related to the hardening function $R(p)$,
- H and m are the viscous modulus and the viscous exponent respectively, and they are related to the viscoplastic related function $Q(\dot{p})$.

For the sake of simplicity, the subscript 0 indicated for the matrix phase is removed since this section is totally devoted to the matrix.

The model is formulated in the framework of thermodynamics. The material state laws are obtained using a Helmholtz potential, whose form is given as follows:

$$\begin{aligned}\rho\psi(\boldsymbol{\varepsilon}, \boldsymbol{\varepsilon}_{v_i}, p, \boldsymbol{\varepsilon}_{\boldsymbol{p}}) = \frac{1}{2}\Big(\boldsymbol{\varepsilon} - \sum_{i=1}^{N} \boldsymbol{\varepsilon}_{v_i} - \boldsymbol{\varepsilon}_{\boldsymbol{p}}\Big) : \mathbb{C}_e : \Big(\boldsymbol{\varepsilon} - \sum_{i=1}^{N} \boldsymbol{\varepsilon}_{v_i} - \boldsymbol{\varepsilon}_{\boldsymbol{p}}\Big) \\ + \sum_{i=1}^{N} \frac{1}{2} \boldsymbol{\varepsilon}_{\boldsymbol{v_i}} : \mathbb{C}_{v_i} : \boldsymbol{\varepsilon}_{\boldsymbol{v_i}} + \int_0^p R(\xi) d\xi,\end{aligned} \tag{39}$$

where $\mathbb{C}_e$ and $\mathbb{C}_{v_i}$ are the elastic stiffness tensor and the viscoelastic stiffness tensor of the i^{th} branch respectively.

Following the standard thermodynamic procedure, the state laws, as well as the relations between state and associated (dual) variables, are obtained and summarized in table 2, where

- $\mathbb{V}_{v_i}$ are the fourth order viscous tensors,
- $\boldsymbol{\sigma}_{\boldsymbol{v_i}}$ are the viscoelastic stresses,
- $\boldsymbol{dev(\sigma)}$ is the deviatoric part of the stress tensor $\boldsymbol{\sigma}$,
- $eq(\boldsymbol{\sigma})$ is the equivalent Von Mises stress.

The viscoplastic part is generated only if the evolution of the multiplier $\dot{\lambda}$ is activated ($\dot{\lambda} > 0$); namely, if the criterion function f becomes positive,

$$f = \mathrm{eq}(\boldsymbol{\sigma}) - R(p) - R_0, \qquad \langle f \rangle_+ = Q(\dot{p}) = H\dot{p}^m. \tag{40}$$

Table 2: Summary of the constitutive equations for the matrix phase in the case of VE-VP response.

Observable state variable	**Associated variable/ State law**	
Total strain $\boldsymbol{\varepsilon}$	$\boldsymbol{\sigma} = \rho\dfrac{\partial\psi}{\partial\boldsymbol{\varepsilon}} = \mathbb{C}_e : \left(\boldsymbol{\varepsilon} - \sum_{i=1}^{N}\boldsymbol{\varepsilon}_{v_i} - \boldsymbol{\varepsilon}_p\right)$	
Internal state variable	**Associated variable/ State law**	**Evolution law**
Viscoelastic strain $\boldsymbol{\varepsilon}_{v_i}$	$-\boldsymbol{\sigma}_{v_i} = \rho\dfrac{\partial\psi}{\partial\boldsymbol{\varepsilon}_{v_i}} = \mathbb{C}_{v_i} : \boldsymbol{\varepsilon}_{v_i} - \boldsymbol{\sigma}$	$\dot{\boldsymbol{\varepsilon}}_{v_i} = \mathbb{V}_{v_i}^{-1} : \boldsymbol{\sigma}_{v_i}$
Viscoplastic strain $\boldsymbol{\varepsilon}_p$	$-\boldsymbol{\sigma} = \rho\dfrac{\partial\psi}{\partial\boldsymbol{\varepsilon}_p}$	$\dot{\boldsymbol{\varepsilon}}_p = \dfrac{3}{2}\dfrac{\boldsymbol{dev}(\boldsymbol{\sigma})}{eq(\boldsymbol{\sigma})}\dot{p}$
Accumulated plastic strain p	$R(p) = \rho\dfrac{\partial\psi}{\partial p} = Kp^n$	$\dot{p} = \dot{\lambda}$

5.3. Identification strategy

As discussed in section 3, the method requires only four parameters valid for all the fiber volume fractions. The four parameters are recalled here. The first one is the ratio $\phi = \frac{c_1}{c_1+c_2}$ where c_1 is the fiber volume fraction and c_2 the coating volume fraction. The other three parameters are the components of the correction tensor $\mathbb{Y}$: $(\gamma^N, \gamma^{ST}, \gamma^{SL})$.

The strategy for evaluating the four parameters is as follows. First, for each volume fraction of fibers and each value of ϕ fixed between 0.5 and 0.9, the set $(\gamma^N, \gamma^{ST}, \gamma^{SL})$ is identified using an optimization algorithm based on the Levenberg-Marquardt technique (Meraghni et al., 2011, 2014). The purpose of the reverse identification method is to find the set of parameters for which the model results coincide (within a tolerance) with the reference full field homogenization results, using a cost function C. The cost function is expressed by the least squares between the new mean field homogenization stress responses σ^{MF} and the FE stress responses σ^{FE}. In the present case, this cost function is

$$C(\gamma^N, \gamma^{ST}, \gamma^{SL}) = \frac{1}{2}\sum_{k=1}^{N_p} w_k\left[\sigma_k^{MF}(\gamma^N, \gamma^{ST}, \gamma^{SL}) - \sigma_k^{FE}\right]^2, \tag{41}$$

where N_p denotes the number of measuring points and w_k a weight given to each of them. Note that

FE analysis on representative cells of the microstructure have been treated as reference solutions for the identification and validation procedure, since it is well-known in the literature that the full field homogenization theory is highly accurate. It is worth noticing that, in long fiber composites, all fields and homogenized properties are independent of the x_3 coordinate (axis parallel to the fibers). Thus, a single row of elements in the direction 3 is sufficient for the full field calculations. Nevertheless, in the current study, a sufficient number of elements through the thickness have been utilized in the full field analyses for illustrative reasons. The obtained results are not altered by this choice.

After the parameters identification, the curves representing the set $(\gamma^N, \gamma^{ST}, \gamma^{SL})$ vs ϕ are plotted for each of the three different volume fractions of fibers utilized for the model identification. The curve corresponding to the EP composite with a critical fiber volume fraction of 50% is illustrated in Fig. 6. The evolution of $(\gamma^N, \gamma^{ST}, \gamma^{SL})$ according to ϕ is explained by the fact that as ϕ

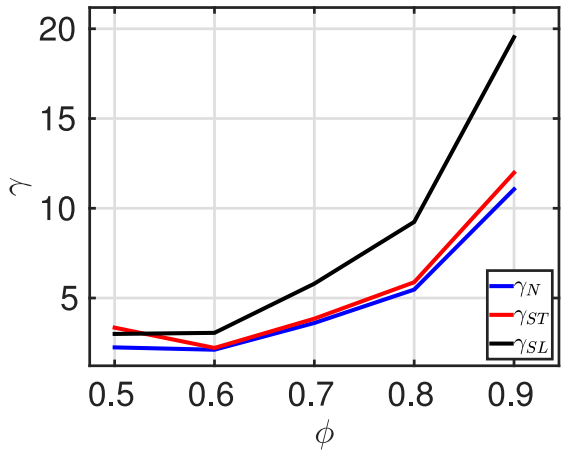

Figure 6: The three component of the correction tensor $(\gamma^N, \gamma^{ST}, \gamma^{SL})$ vs ϕ for a composite consisting of an EP matrix reinforced by 50% of fibers. For values of ϕ exceeding 0.8 an overshoot of the inelastic strain gradient between the matrix and the coating is noticed. Inversely, for values of ϕ inferior to 0.6 the matrix tends to be annihilated.

increases, the volume fraction of the coating $c_2 = \frac{c_1}{\phi} - c_1$ decreases. Thus, the three components of the correction tensor must be increased to compensate the loss of inelastic strain induced by the decrease of c_2. In addition, it can be observed that the values of the correction tensor components $(\gamma^N, \gamma^{ST}, \gamma^{SL})$ are quite close.

For a proper choice of ϕ, one should keep in mind that the higher the value of ϕ (i.e. low coating volume fraction), the higher the strain concentration in a reduced volume of coating. Hence, an excessive difference between the average inelastic strain in the matrix and that in the coating is observed for values of ϕ exceeding 0.8. This overshoot of the inelastic strain gradient can lead to numerical instabilities. Conversely, a low value of ϕ (i.e. high coating volume) annihilates the matrix. Moreover, an average of the set (γ^N, γ^{ST}, γ^{SL}) was computed on the three fiber volume fractions utilized for the identification in order to obtain a single set valid for all fiber volume fractions.

The simulations performed for the identification and the validation of the model have been carried out on a single macroscopic material point. For infinitely long fibers parallel to the third direction, the parameters are optimized from three uniaxial load/unload tensile tests: transverse tensile (1-1), in-plane shear (1-2) and out-of-plane shear (1-3). Each component of the correction tensor $\mathbb{Y}$ can be identified independently for each of the three loading directions (Figs. 7a-7c). Furthermore, Figs. 7d-7f present contour plots of the plastic strain in the matrix. Therefore, Fig. 7 highlights the effect of the corresponding correction tensor $\mathbb{Y}$ on the size of the concentration zone and the amplitude of the inelastic strain.

5.4. Identification and validation

To demonstrate the model's capabilities to predict rate-independent as well as rate-dependent behavior of composites, two rheological configurations are studied: an EP composite and a VE-VP composite. Figs. 8-17 illustrate comparisons between three different homogenization models: the classical mean field homogenization model, the mean field homogenization model modified to take into account the coating, and the reference full field homogenization model. In the examples utilized to identify and validate the modified Mori-Tanaka TFA model, four non-monotonic loading conditions are applied: transverse tensile (1-1), in-plane shear (1-2) and out-of-plane shear (1-3), as well as non-proportional multi-axial loading paths, in which a transverse tension is combined to an in-plane shear. Moreover, average local strain fields per phase obtained by the three methods, are examined. Hereafter, the acronyms CMFH, MMFH and FFH stand for the Classical Mean Field Homogenization, the Modified Mean Field Homogenization and the reference Full

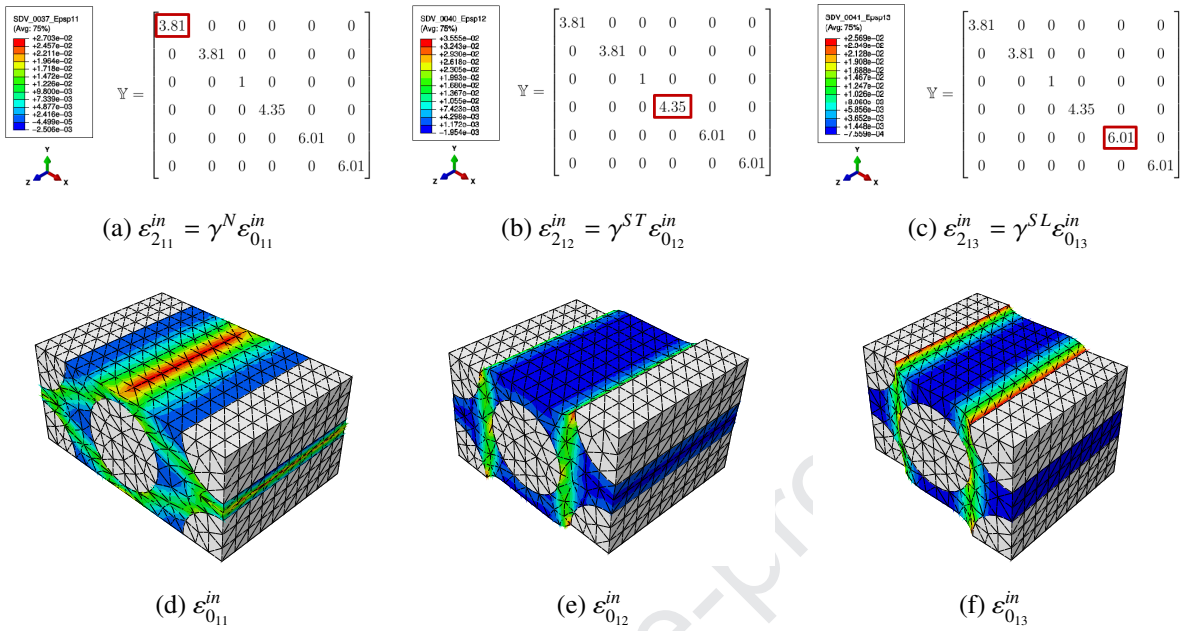

Figure 7: Comparison between the size of the concentration zone of the inelastic strain in the matrix ε^{in}_{0} and the value of each component of the correction tensor $\mathbb{Y}$, for an elastoplastic composite reinforced with 50% of long fibers directed in direction z, for three different loading paths: transversal tension (7d), in-plane shear (7e) and out-of-plane shear (7f).

Field Homogenization method, respectively.

5.4.1. Identification results for elastoplastic composites

Using the identification strategy described above, the parameters governing the proposed constitutive model have been identified on the elastoplastic composite presented in section 5.2. The ratio ϕ is chosen equal to 0.7. For this ϕ, the optimization procedure for 10%, 30% and 50% fiber volume fractions lead to three different sets of parameters, summarized in table 3. Since the obtained values per parameter are relatively close, the final identified parameters are considered to be their mean values, i.e. $\gamma^{N} = 3.81$, $\gamma^{ST} = 4.35$, $\gamma^{SL} = 6.01$.

Fig. 8 represents the simulated curves utilized for the identification of the global behavior of an EP matrix reinforced with 50% of fibers in direction 3, for three uniaxial loading paths. It is worth mentioning that the slight "kinematic effect" at the end of the unloading part of figure 8a in the classical Mori-Tanaka model is due to the fact that the matrix phase in the composite is in

Table 3: Identified parameters γ^N, γ^{ST} and γ^{SL} for $\phi = 0.7$ and three different fiber volume fractions.

volume fraction	γ^N	γ^{ST}	γ^{SL}
10%	3.98	4.74	6.17
30%	3.86	4.48	6.07
50%	3.61	3.85	5.81

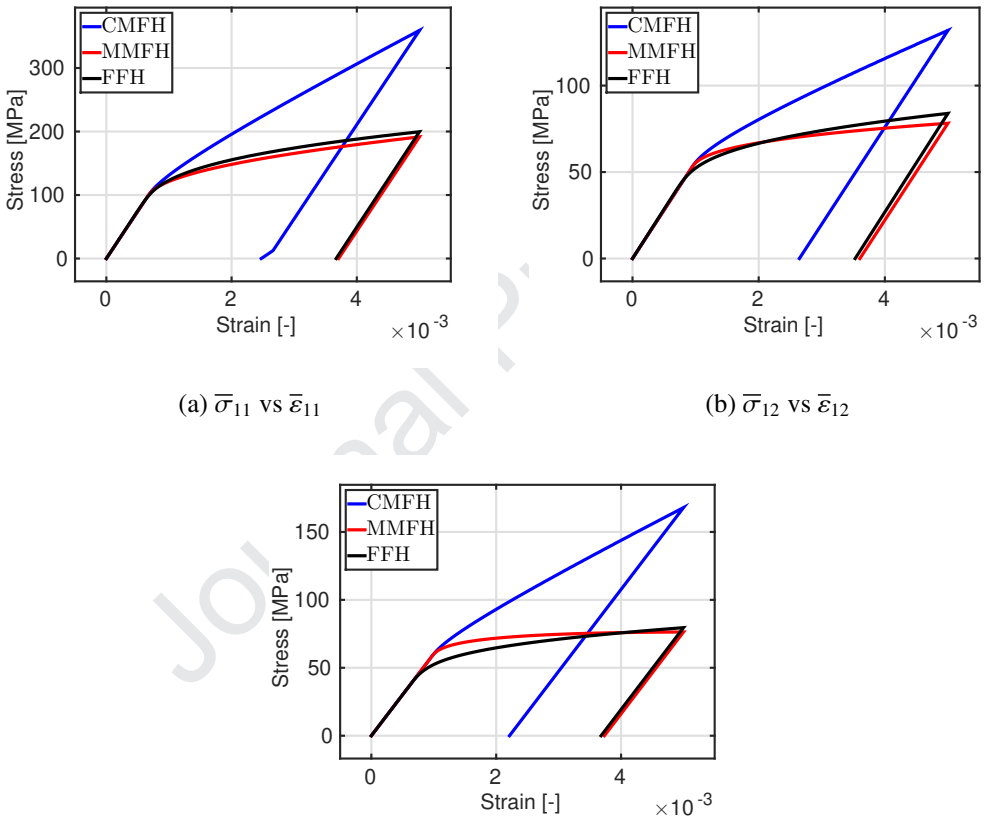

(a) $\overline{\sigma}_{11}$ vs $\overline{\varepsilon}_{11}$

(b) $\overline{\sigma}_{12}$ vs $\overline{\varepsilon}_{12}$

(c) $\overline{\sigma}_{13}$ vs $\overline{\varepsilon}_{13}$

Figure 8: Load/Unload tensile tests on an EP composite reinforced by 50% of long fibers for the three different loading paths: the transversal tension (1-1), the in-plane shear (1-2) and the out-of-plane shear (1-3) (identification). Comparison between the classical mean field homogenization model (CMFH), the modified mean field homogenization model (MMFH) and the reference full field homogenization model (FFH).

triaxial condition and during unloading it enters into compression in direction 1. The developed von Mises stress is sufficient to activate the isotropic hardening in the unloading stage. This in turn appears as pseudo-kinematic effect in the composite. The obtained results demonstrate the model's ability to capture properly the unrecoverable plastic strain after unloading, even for a critical fiber volume fraction of 50%.

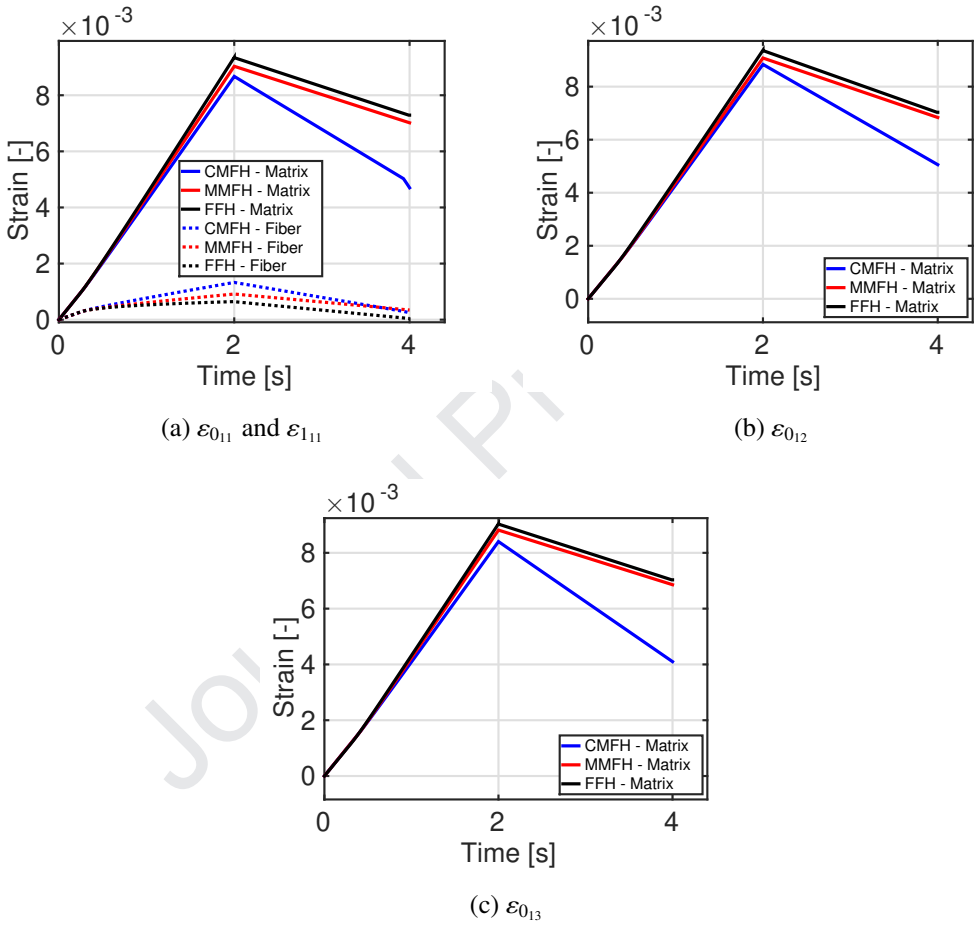

(a) $\varepsilon_{0_{11}}$ and $\varepsilon_{1_{11}}$ (b) $\varepsilon_{0_{12}}$

(c) $\varepsilon_{0_{13}}$

Figure 9: Load/Unload tensile tests on an EP matrix reinforced by 50% of long fibers. Averaged local strain in the matrix for the three different loading paths: $\varepsilon_{0_{11}}$ for the transverse tension, $\varepsilon_{0_{12}}$ for the in-plane shear and $\varepsilon_{0_{13}}$ for the out-of-plane shear; averaged local strain in the fiber for transverse tension $\varepsilon_{1_{11}}$. Comparison between the classical mean field homogenization model (CMFH), the modified mean field homogenization model (MMFH) and the reference full field homogenization model (FFH).

Moreover, the per phase average strain fields are depicted in Fig. 9. For the full field homogenization analysis, the average matrix or fiber fields are computed from the volume average of

the fields obtained at each element of the FE unit cell. For the new mean field homogenization method, the strain fields are evaluated from the volume average of the total matrix comprising both the matrix and the fictitious coating. A good agreement is observed between the average strain in the matrix phase predicted by the new mean field homogenization method and the average matrix strain obtained by FE simulations (Fig. 9). In Fig. 9a, the levels of strain in the fibers are so low that the differences observed are not really revealing.

Figs. 10 and 11 demonstrate the local plastic strain and local stress fields respectively inside the unit cell at the peak of the first loading case (transversal tension). The comparison between the full field (FFH) and the modified mean field (MMFH) homogenization model results reveal that the proposed methodology captures satisfactorily the local fields per phase. As shown in Fig. 11, the MMFH gives an over-prediction on the fiber stress (333 MPa as opposed to approximately 250 MPa). This issue could be potentially resolved if one considers more than one coating layer. In the latter case though, the computation of the $\mathbb{Y}$ tensor per layer becomes a more complicated task, requiring more advanced parameter identification techniques. As a conclusion, it can be stated that the modified Mori-Tanaka TFA method, integrating the presence of a pseudo-coating, is able to predict quite accurately both the macroscopic and microscopic responses of nonlinear composites reinforced with long elastic fibers.

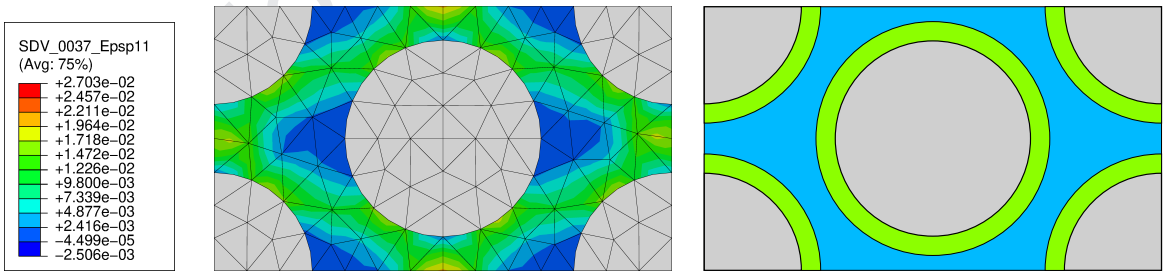

(a) FFH (b) MMFH

Figure 10: Transversal tension (1-1) test on an EP matrix reinforced by 50% of long fibers. Comparison of local plastic strain fields (component 11) at the peak loading between the reference full field homogenization model (FFH) and the modified mean field homogenization model (MMFH).

Fig. 12 represents the stress-strain responses of a transverse traction for the three different volume fractions utilized for the identification (10%, 30% and 50%). It shows the ability of the new

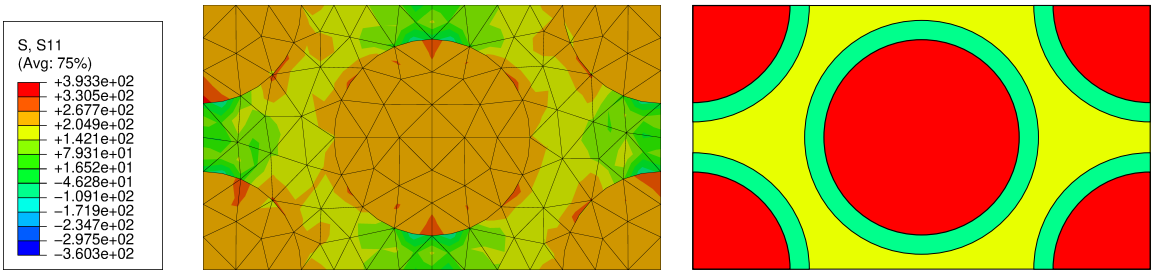

(a) FFH (b) MMFH

Figure 11: Transversal tension (1-1) test on an EP matrix reinforced by 50% of long fibers. Comparison of local stress fields (component 11) at the peak loading between the reference full field homogenization model (FFH) and the modified mean field homogenization model (MMFH).

model to capture properly the EP composite behavior for a wide range of fiber volume fractions. Nonetheless, the quality of the new model's predictions declines slightly when increasing the volume fraction of the stiffer elastic long fibers. Actually, it is known in the literature that mean field homogenization models become less accurate as the volume fraction of inclusions increases.

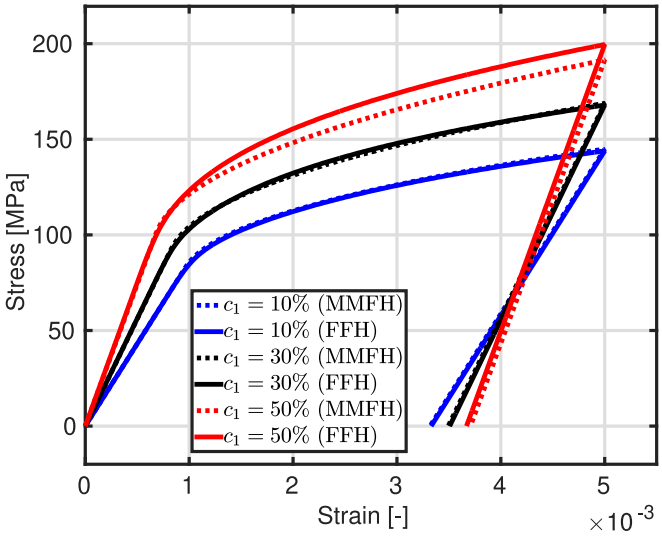

Figure 12: Transverse traction tests with a load/unload path, on EP composites reinforced by different volume fractions of long fibers: 10%, 30%, and 50% (identification). Comparison between the modified mean field homogenization model (MMFH) and the reference full field homogenization model (FFH).

5.4.2. *Validation results on elastoplastic composites*

Validation on different volume fractions

Figs. 13-14 show the simulated curves used for the validation of the global behavior of an EP matrix reinforced with 20% and 40% of fibers oriented in direction 3. It is recalled that these two volume fractions are not utilized in the identification procedure. The good agreement between the modified Mori-Tanaka TFA and the FE results validates the previously identified parameters. It also confirms that the new model is able to predict properly the EP composite behavior for a wide range of fiber volume fractions and for three different loading paths.

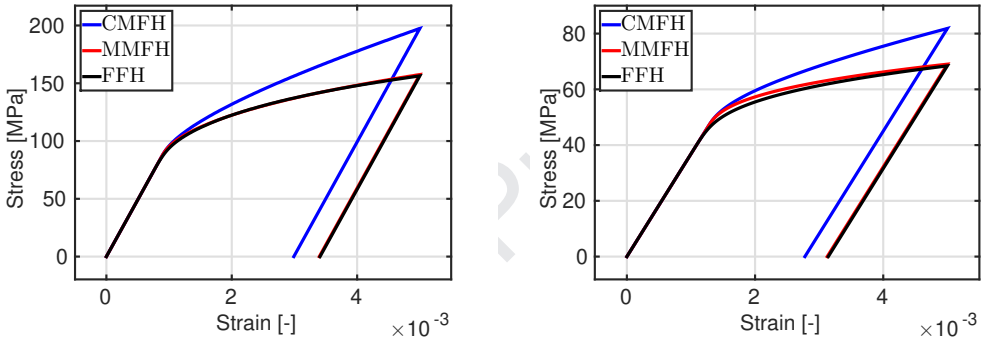

(a) $\overline{\boldsymbol{\sigma}}_{11}$ vs $\overline{\boldsymbol{\varepsilon}}_{11}$ (b) $\overline{\boldsymbol{\sigma}}_{12}$ vs $\overline{\boldsymbol{\varepsilon}}_{12}$

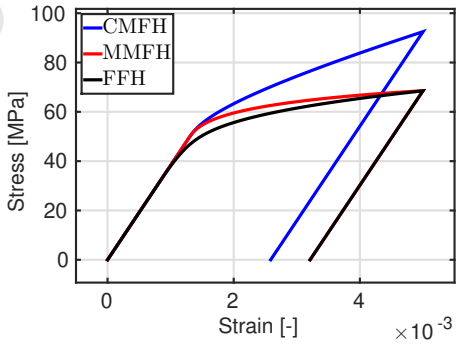

(c) $\overline{\boldsymbol{\sigma}}_{13}$ vs $\overline{\boldsymbol{\varepsilon}}_{13}$

Figure 13: Load/Unload tensile tests on an EP composite reinforced by 20% of long fibers for the three different loading paths: the transversal tension (1-1), the in-plane shear (1-2) and the out-of-plane shear (1-3) (validation). Comparison between the classical mean field homogenization model (CMFH), the modified mean field homogenization model (MMFH) and the reference full field homogenization model (FFH).

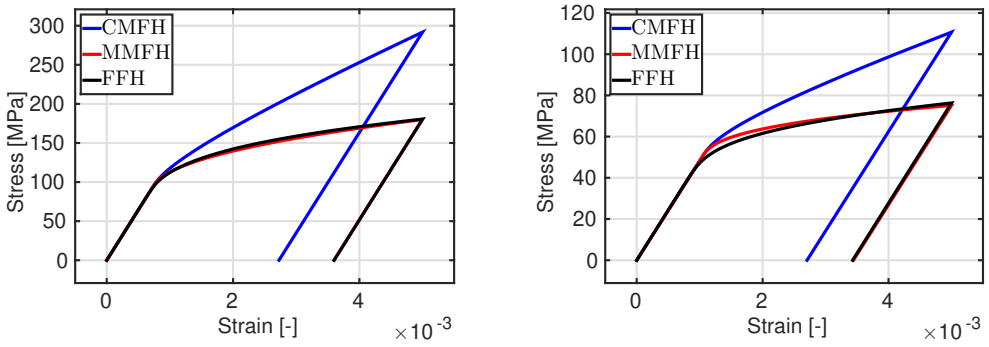

(a) $\overline{\boldsymbol{\sigma}}_{11}$ vs $\overline{\boldsymbol{\varepsilon}}_{11}$

(b) $\overline{\boldsymbol{\sigma}}_{12}$ vs $\overline{\boldsymbol{\varepsilon}}_{12}$

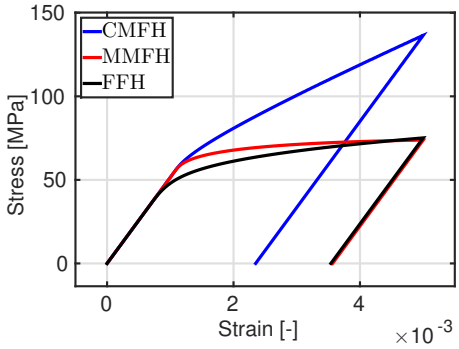

(c) $\overline{\boldsymbol{\sigma}}_{13}$ vs $\overline{\boldsymbol{\varepsilon}}_{13}$

Figure 14: Load/Unload tensile tests on an EP composite reinforced by 40% of long fibers for the three different loading paths: the transversal tension (1-1), the in-plane shear (1-2) and the out-of-plane shear (1-3) (validation). Comparison between the classical mean field homogenization model (CMFH), the modified mean field homogenization model (MMFH) and the reference full field homogenization model (FFH).

Validation on non proportional multi-axial loading path

In the following simulation, the EP composite is subjected to a transverse tension (index 11) combined to an in-plane shear (index 12), which are applied through a non-proportional loading path (Fig. 15a):

1. During the first 5 seconds ($t_1 = 5s$), ε_{11} increases linearly until 0.002, while ε_{12} is held null.
2. From t_1 to $2t_1$, ε_{11} is held constant, while ε_{12} increases linearly until 0.001.
3. From $2t_1$ to $3t_1$, both σ_{11} and σ_{12} decrease linearly until 0.0 MPa.

The results of these simulations are presented in Fig. 15b through the transverse tension stress σ_{11} and the in-plane shear stress σ_{12} responses. The overall good agreements between the simulated curves using the new model and the FE reference results demonstrate the capabilities of the model to describe the correct anisotropic response of the composite since the model predictions are generally very satisfying for nonlinear rate-independent composites.

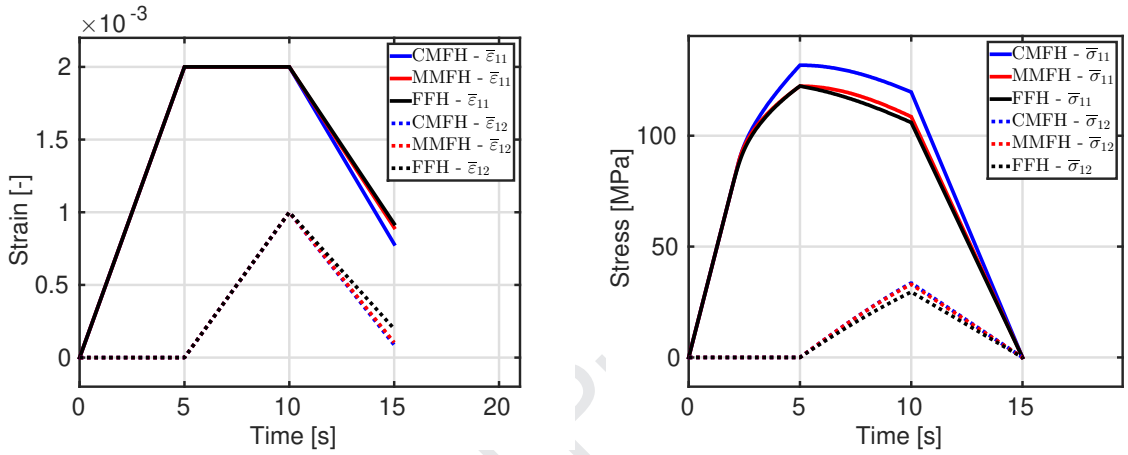

(a) Applied strain ($\overline{\varepsilon}_{11}$ and $2\overline{\varepsilon}_{12}$) vs time

(b) Stress responses ($\overline{\sigma}_{11}$ and $\overline{\sigma}_{12}$) vs time

Figure 15: Complex non-proportional combined transverse tension (1-1) and in-plane shear (1-2) tests on a EP composite reinforced by 20% of long fibers. Comparison between the classical mean field homogenization model (CMFH), the modified mean field homogenization model (MMFH) and the reference full field homogenization model (FFH). It is recalled that the unloading stage is stress controlled.

5.4.3. Identification and validation on VE-VP composites

Identification

For the VE-VP composite presented in section 5.2, the model's parameters have been identified in the same manner as discussed in section 5.3. The ratio ϕ is chosen equal to 0.57 and the identified parameters values are : $\gamma^N = 2.5$, $\gamma^{ST} = 2.64$, $\gamma^{SL} = 3.7$. Fig. 16 illustrates the simulations performed for the identification of the global behavior of the VE-VP matrix reinforced with 20% of long fibers oriented in direction 3, for three uniaxial loading paths, at a strain rate of 0.035 s^{-1}.

Validation on non proportional multi-axial loading path

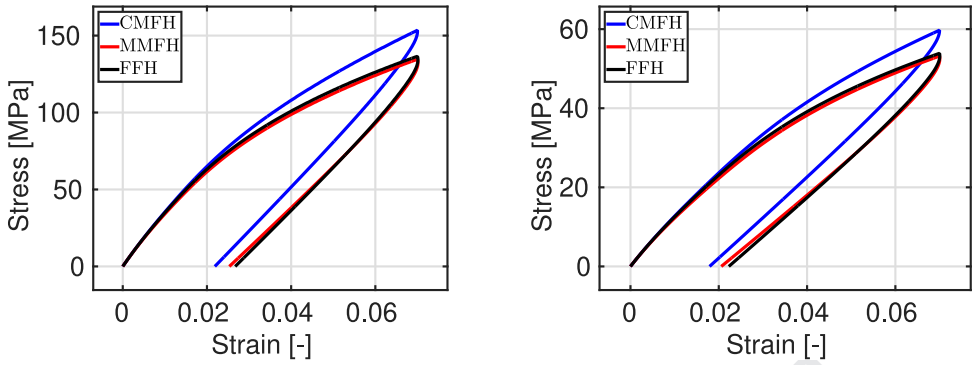

(a) $\overline{\sigma}_{11}$ vs $\overline{\varepsilon}_{11}$

(b) $\overline{\sigma}_{12}$ vs $\overline{\varepsilon}_{12}$

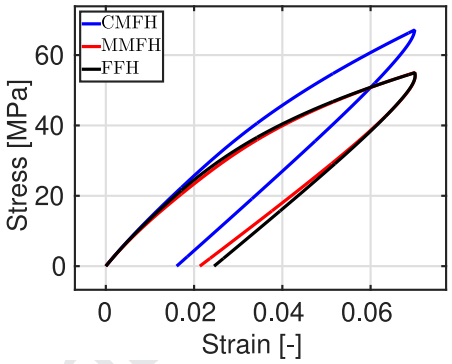

(c) $\overline{\sigma}_{13}$ vs $\overline{\varepsilon}_{13}$

Figure 16: Load/Unload tensile tests on a VE-VP composite reinforced by 20% of long fibers for the three different loading paths: the transversal tension (1-1), the in-plane shear (1-2) and the out-of-plane shear (1-3), at a strain rate of 0.035 s^{-1} (identification). Comparison between the classical mean field homogenization model (CMFH), the modified mean field homogenization model (MMFH) and the reference full field homogenization model (FFH).

In the following simulations, the VE-VP composite is subjected to a transverse tension (index 11) combined to an in-plane shear (index 12), which are applied through a non-proportional loading path (Fig. 17a):

1. From 0 s to t_1, ε_{11} increases linearly until 0.002, while ε_{12} is held null.
2. From t_1 to $2t_1$, ε_{11} is held constant, while ε_{12} increases linearly until 0.001.
3. From $2t_1$ to $3t_1$, both ε_{11} and ε_{12} are held constant.
4. From $3t_1$ to $4t_1$, both σ_{11} and σ_{12} decrease linearly until 0.0 MPa.

This complex loading path is performed under different strain rates, emphasizing the global rate effect due to viscoelasticity and viscoplasticity. The following strain rates are chosen (Figs. 17a, 18a and 19a):

1. First loading strain rates : $\dot{\varepsilon}_{11} = 0.004\ s^{-1}$ and $\dot{\varepsilon}_{12} = 0.0027\ s^{-1}$ ($t_1 = 0.1s$).
2. Second loading strain rates : $\dot{\varepsilon}_{11} = 0.012\ s^{-1}$ and $\dot{\varepsilon}_{12} = 0.008\ s^{-1}$ ($t_1 = 5s$).
3. Third loading strain rates : $\dot{\varepsilon}_{11} = 0.6\ s^{-1}$ and $\dot{\varepsilon}_{12} = 0.4\ s^{-1}$ ($t_1 = 15s$).

Long-term stress relaxation is illustrated by the decrease of σ_{11} and σ_{12} when both ε_{11} and ε_{12} are held constant (step 3, Fig. 17b).

Figs. 17b, 18b and 19b show the stress response for the composite predicted by the new approach, compared to the classical mean field homogenization and the full field homogenization (reference). The effect of the non proportional loading (tension-shear) is demonstrated by the combination of i) the plasticity-type criterion for the balance of the stresses expressed in the effective stress and ii) the viscous relaxation when one or both strains are held constant. The proposed model, based on a modified mean field homogenization, captures properly the rate effect, since it gives satisfactory results for the three different strain rates. It is pointed out that the proposed homogenization approach gives predictions very close of the FE results, while significantly reducing the computational time. Indeed, for the simulation presented in Fig. 19, the computational time of the FE analysis is around 15 minutes whereas for the new mean field model, the computational time is less than one second. Consequently, the model is also valid for rate-dependent composite behavior.

5.5. Discussion

The first part of the numerical simulations presented in this manuscript is carried out on an EP matrix reinforced with long fibers. The modified Mori-Tanaka TFA predictions were compared to the classical Mori-Tanaka TFA ones and the FE simulations on unit cells. In general, the modified mean field homogenization results were found to be satisfying, for the non-monotonic and non-proportional multi-axial loading paths. Moreover, five different fiber volume fractions have been tested on EP composites, and the accuracy of the results remains good when increasing the volume

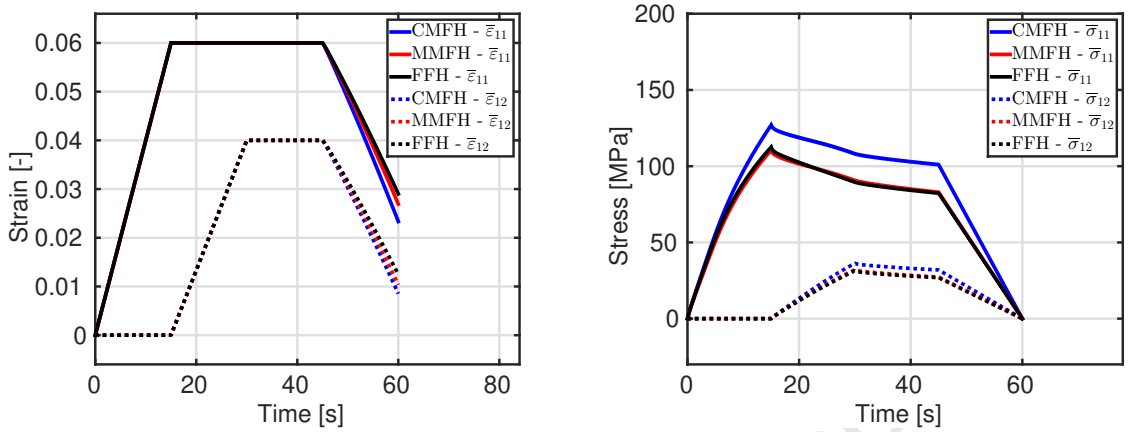

(a) Applied strain ($\overline{\varepsilon}_{11}$ and $2\overline{\varepsilon}_{12}$) vs time

(b) Stress responses ($\overline{\sigma}_{11}$ and $\overline{\sigma}_{12}$) vs time

Figure 17: Complex non-proportional combined transverse tension (1-1) and in-plane shear (1-2) virtual test on a VE-VP composite reinforced by 20% of long fibers, at the strain rates $\dot{\varepsilon}_{11} = 0.004\ s^{-1}$ and $\dot{\varepsilon}_{12} = 0.0027\ s^{-1}$. Comparison between the classical mean field homogenization model (CMFH), the modified mean field homogenization model (MMFH) and the reference full field homogenization model (FFH). It is recalled that the unloading stage is stress controlled.

fraction of the stiffer elastic inclusions, even for a critical volume fraction of 50% (subsection 5.4.1). It should be pointed out that under certain extreme conditions (for instance, very low plastic hardening of the matrix phase), instability modes can take place. Such phenomena exceed the capabilities of a first order homogenization scheme. Even the full field computations used in this work are unable to capture such mechanisms, unless higher order terms are accounted for. In Mori-Tanaka homogenization strategies, where only average fields per phase are computed, information about gradient effects can be obtained using special techniques (Wu et al., 2013b). The current model does not compute strain gradients, and hence it cannot capture size effects.

The second part of the simulations is performed on a VE-VP matrix reinforced with long fibers in order to prove the model's capabilities to predict the rate-dependent behavior of composites. As mentioned in section 2, the paper carried out by Miled et al. (2013) proposes a mean field homogenization approach with an isotropization of the anisotropic tangent modulus, to model inclusion-reinforced viscoelastic-viscoplastic composites. It was found that compared to FE simulations, their results worsen when decreasing the strain rate. In the study presented in this manuscript,

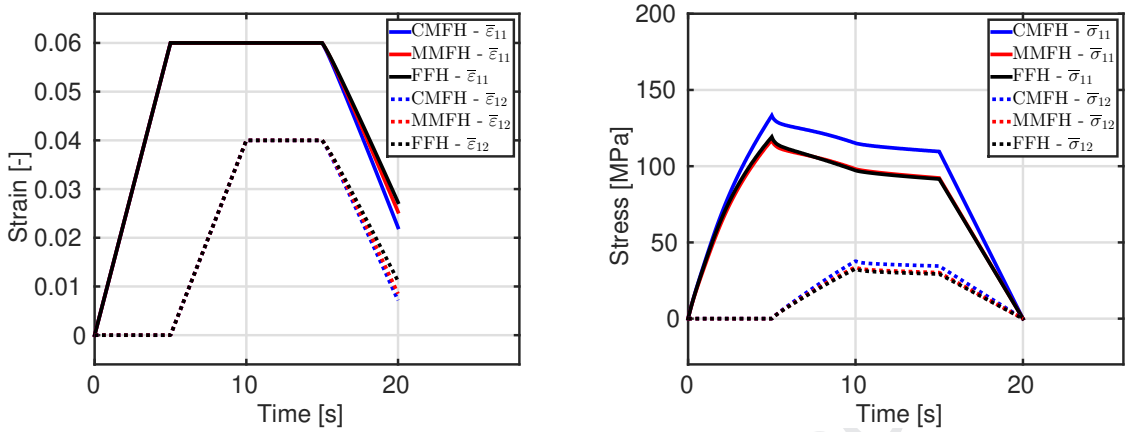

(a) Applied strain ($\overline{\varepsilon}_{11}$ and $2\overline{\varepsilon}_{12}$) vs time

(b) Stress responses ($\overline{\sigma}_{11}$ and $\overline{\sigma}_{12}$) vs time

Figure 18: Complex non-proportional combined transverse tension (1-1) and in-plane shear (1-2) virtual test on a VE-VP composite reinforced by 20% of long fibers, at the strain rates $\dot{\varepsilon}_{11} = 0.012\ s^{-1}$ and $\dot{\varepsilon}_{12} = 0.008\ s^{-1}$. Comparison between the classical mean field homogenization model (CMFH), the modified mean field homogenization model (MMFH) and the reference full field homogenization model (FFH). It is recalled that the unloading stage is stress controlled.

non-proportional multi-axial loading have been simulated on VE-VP composites on three different strain rates (subsection 5.4.3). It has been shown that the Mori Tanaka TFA with virtual coatings is valid whatever the strain rate tested. Furthermore, although predictions of Miled et al. (2013) model are generally acceptable, it is observed that the results on VE-VP composites are much less accurate than those of E-VP, even for fibers with an aspect ratio of 100 (long fibers). In their opinion, the problem arises from the VE part of the response, and from the fact that in VE-VP there are different relaxation times associated with both the VE and VP parts, while in E-VP only VP relaxation times are present. In the simulations presented here, two different relaxation times are utilized. Moreover, the VE strain in the matrix is not negligible compared to the VP one, and yet, the results are satisfying for all the loading paths tested.

5.6. Conclusions and perspectives

In this paper, a modified version of a mean field multi-scale strategy, using TFA framework and Mori-Tanaka scheme, has been proposed to predict the overall behavior of long fiber reinforced

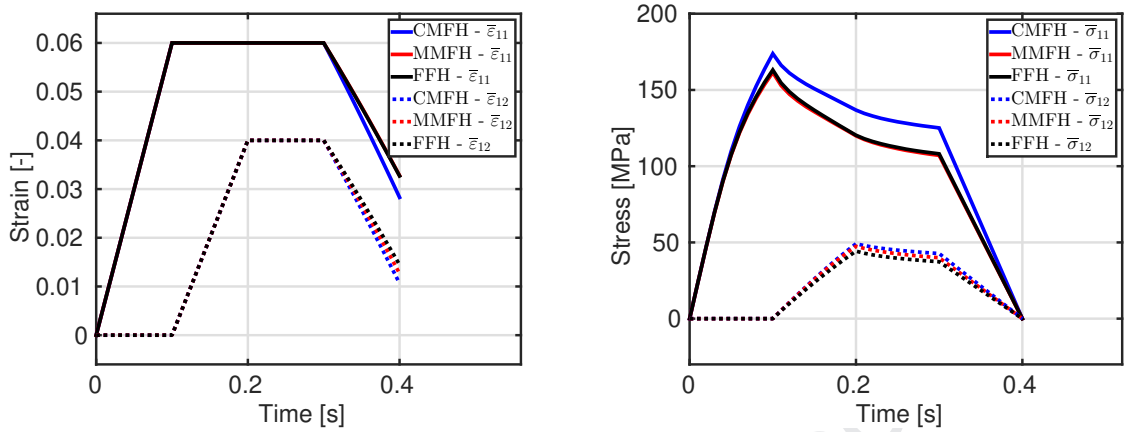

(a) Applied strain ($\overline{\varepsilon}_{11}$ and $2\overline{\varepsilon}_{12}$) vs time

(b) Stress responses ($\overline{\sigma}_{11}$ and $\overline{\sigma}_{12}$) vs time

Figure 19: Complex non-proportional combined transverse tension (1-1) and in-plane shear (1-2) virtual test on a VE-VP composite reinforced by 20% of long fibers, at the strain rates $\dot{\varepsilon}_{11} = 0.6\ s^{-1}$ and $\dot{\varepsilon}_{12} = 0.4\ s^{-1}$. Comparison between the classical mean field homogenization model (CMFH), the modified mean field homogenization model (MMFH) and the reference full field homogenization model (FFH). It is recalled that the unloading stage is stress controlled.

elastoplastic or viscoelastic-viscoplastic composites. Motivated by observations from full field computations in RVEs, an additional layer between the matrix and the fiber, named coating, has been integrated in order to take into account the high inelastic strain concentration around the fibers. To integrate the nonlinear behavior of the matrix phase into the multi-scale scheme, a return mapping algorithm has been implemented in the ABAQUS FE software via a user-defined constitutive law coded in Fortran.

The model has been identified and extensively validated using finite element simulations in RVEs, considered as reference solutions, under load/unload and non proportional multi-axial loading paths. The main strengths of this method are as follows. First, the small number of parameters to identify, namely three parameters for nonlinear matrix reinforced by infinitely long cylindrical fibers, makes the method easy to implement. Moreover, the identified parameters are valid for a wide range of reinforcement volume fractions, allowing for the method to be adopted fast in parametric studies. It is also suitable for both rate independent and rate dependent behavior, as illustrated by the various studies in section 5. In addition, the proposed multi-scale approach

is able to predict the global rate effect for a unique set of identified properties, as shown by the validation tests on rate-dependent composites, performed at three different strain rates. An added important advantage of the presented strategy is that it predicts both the macroscopic and the averaged microscopic responses in each phase of the composite. Finally, it provides predictions very close to those of the FE results considering the corresponding RVEs, with significant reduction of the computational cost. The latter advantage is essential for structural industrial applications.

With regard to the perspectives, the current work can be adopted also in the case of short fiber composites, considering appropriate diameter to length ratios. In such cases, one should consider the possibility that additional parameters may be required for identifying the correction tensor $\mathbb{Y}$. Moreover, the multi-scale approach can be extended to composites undergoing damage mechanisms (matrix and/or interfacial damage) in addition to viscoelasic-viscoplasic behavior. Such constitutive response is often the case for thermoplastic polymer based composites.

Aboudi, J., 2005. Micromechanically established constitutive equations for multiphase materials with viscoelastic-viscoplastic phases. Mechanics of Time-Dependent Materials 9 (2-3), 121–145.

Benveniste, Y., 1987. A new approach to the application of Mori-Tanaka's theory in composite materials. Mechanics of Materials 6, 147–157.

Berbenni, S., Cherkaoui, M., 2010. Homogenization of multicoated inclusion-reinforced linear elastic composites with eigenstrains: Application to thermoelastic behavior. Philosophical Magazine 90 (22), 3003–3026.

Bilger, N., Auslender, F., Bornert, M., Moulince, H., Zaoui, A., 2007. Bounds and estimates for the effective yield surface of porous media with a uniform or a nonuniform distribution of voids. European Journal of Mechanics A/Solids 26, 810–836.

Boudet, J., Auslender, F., Bornert, M., Lapusta, Y., 2016. An incremental variational formulation for the prediction of the effective work-hardening behavior and field statistics of elasto-(visco)plastic composites. International Journal of Solids and Structures 83, 90–113.

Brassart, L., Stainier, L., Doghri, I., Delannay, L., 2012. Homogenization of elasto-(visco) plastic composites based on an incremental variational principle. International Journal of Plasticity 36, 86–112.

Cavalcante, M. A. A., Pindera, M.-J., 2013. Finite-volume enabled transformation field analysis of periodic materials. International Journal of Mechanics and Materials in Design 9, 153–179.

Chaboche, J.-L., Kanoute, P., 2003. Sur les approximations ≪isotrope≫ et ≪anisotrope≫ de l'opérateur tangent pour les méthodes tangentes incrémentale et affine. Comptes Rendus Mécanique 331, 857–864.

Chaboche, J.-L., Kanoute, P., Roos, A., 2005. On the capabilities of mean-field approaches for the description of plasticity in metal matrix composites. International Journal of Plasticity 21, 1409–1434.

Chaboche, J.-L., Kruch, S., Maire, J., Pottier, T., 2001. Towards a micromechanics based inelastic and damage modeling of composites. International Journal of Plasticity 17, 411–39.

Charalambakis, N., Chatzigeorgiou, G., Chemisky, Y., Meraghni, F., 2018. Mathematical homogenization of inelastic dissipative materials: A survey and recent progress. Continuum Mechanics and Thermodynamics 30 (1), 1–51.

Chatzigeorgiou, G., Charalambakis, N., Chemisky, Y., Meraghni, F., 2018. Thermomechanical Behavior of Dissipative Composite Materials. ISTE Press - Elsevier, London.

Chatzigeorgiou, G., Meraghni, F., 2019. Elastic and inelastic local strain fields in composites with coated fibers or particles: Theory and validation. Mathematics and Mechanics of Solids, in press.

Czarnota, C., Kowalczyk-Gajewska, K., Salahouelhadj, A., Martiny, M., Mercier, S., 2015. Modeling of the cyclic behavior of elastic-viscoplastic composites by the additive tangent Mori-Tanaka approach and validation by finite element calculations. International Journal of Solids and Structures 56-57, 96–117.

Despringre, N., 2015. Analyse et modélisation des mécanismes d'endommagement et de déformation en fatigue multiaxiale de matériaux composites : polyamide renforcée par des fibres courtes. Ph.D. thesis, Ecole Nationale Supérieure d'Arts et Métiers - ENSAM.

Desrumaux, F., Meraghni, F., Benzeggagh, M.-L., 2001. Generalised Mori-Tanaka Scheme to Model Anisotropic Damage Using Numerical Eshelby Tensor. Journal of Composite Materials 35 (7), 603–624.

Doghri, I., Adam, L., Bilger, N., 2010. Mean-field homogenization of elasto-viscoplastic composites based on a general incrementally affine linearization method. International Journal of Plasticity 26, 219–238.

Doghri, I., Brassart, L., Adam, L., Gerard, J.-S., 2011. A second-moment incremental formulation for the mean-field homogenization of elasto-plastic composites. International Journal of Plasticity 27, 352–371.

Doghri, I., Ouaar, A., 2003. Homogenization of two-phase elasto-plastic composite materials and structures: Study of tangent operators, cyclic plasticity and numerical algorithms. International Journal of Solids and Structures 40, 1681–1712.

Dondeti, P., Paquet, D., Ghosh, S., 2012. A rate-dependent homogenization based continuum plasticity-damage (HCPD) model for dendritic cast aluminum alloys. Engineering Fracture Mechanics 89, 75–97.

Dvorak, G.-J., 1992. Transformation field analysis of inelastic composite materials. Proceedings of the Royal Society of London A 437, 311–327.

Dvorak, G.-J., Bahel-El-Din, Y., Wafa, A., 1994. Implementation of the transformation field analysis for inelastic composite materials. Computational Mechanics 14, 201–228.

Dvorak, G.-J., Benveniste, Y., 1992. On transformation strains and uniform fields in multiphase elastic media. Proceedings of the Royal Society of London A 437, 291–310.

Eshelby, J.-D., 1957. The determination of the elastic field of an ellipsoidal inclusion, and related problems. Proceedings of the Royal Society of London A 241, 376–396.

Fournier, B., Sauzay, M., Pineau, A., 2011. Micromechanical model of the high temperature cyclic behavior of 9-

12%Cr martensitic steels. International Journal of Plasticity 27, 1803–1816.

Fritzen, F., Forest, S., Böhlke, T., Kondo, D., Kanit, T., 2012. Computational homogenization of elasto-plastic porous metals. International Journal of Plasticity 29, 102–119.

Gavazzi, A.-C., Lagoudas, D.-C., 1990. On the numerical evaluation of eshelby's tensor and its application to elasto-plastic fibrous composites. Computational Mechanics 7, 13–19.

Geers, M. G. D., Kouznetsova, V. G., Brekelmans, W. A. M., 2010. Multi-scale computational homogenization: Trends and challenges. Journal of Computational and Applied Mathematics 234 (7), 2175–2182.

Guo, S., Kang, G., Zhang, J., 2011. Meso-mechanical constitutive model for ratchetting of particle-reinforced metal matrix composites. International Journal of Plasticity 27, 1896–1915.

Hill, R., 1965. A self-consistent mechanics of composite materials. Journal of the Mechanics and Physics of Solids 13, 231.

Jiang, T., Shao, J.-F., 2009. On the incremental approach for nonlinear homogenization of composite and influence of isotropization. Computational Materials Science 46, 447–451.

Kanouté, P., Boso, D. P., Chaboche, J. L., Schrefler, B. A., 2009. Multiscale methods for composites: a review. Archives of Computational Methods in Engineering 16, 31–75.

Kattan, P., Voyiadjis, G., 1993. Overall damage and elastoplastic deformation in fibrous metal matrix composites. International Journal of Plasticity 9, 931–949.

Kotha, S., Ozturk, D., Ghosh, S., 2019. Parametrically homogenized constitutive models (PHCMs) from micromechanical crystal plasticity FE simulations, part I: Sensitivity analysis and parameter identification for Titanium alloys. International Journal of Plasticity 120, 296–319.

Kruch, S., Chaboche, J.-L., 2011. Multi-scale analysis in elasto-viscoplasticity coupled with damage. International Journal of Plasticity 27, 2026–2039.

Lagoudas, D.-C., Gavazzi, A.-C., Nigam, H., 1991. Elastoplastic behavior of metal matrix composites based on incremental plasticity and the mori-tanaka averaging scheme. Computational Mechanics 8, 193–203.

Lahellec, N., Suquet, P., 2007. On the effective behavior of nonlinear inelastic composites: I. Incremental variational principles. Journal of the Mechanics and Physics of Solids 55 (9), 1932–1963.

Li, J., Romero, I., Segurado, J., 2019. Development of a thermo-mechanically coupled crystal plasticity modeling framework: Application to polycrystalline homogenization. International Journal of Plasticity 119, 313–330.

Mahnken, R., Schneidt, A., Antretter, T., 2009. Macro modelling and homogenization for transformation induced plasticity of a low-alloy steel. International Journal of Plasticity 25, 183–204.

Mareau, C., Favier, V., Weber, B., Galtier, A., Berveiller, M., 2012. Micromechanical modeling of the interactions between the microstructure and the dissipative deformation mechanisms in steels under cyclic loading. International Journal of Plasticity 32-33, 106–120.

Matsuda, T., Kanamaru, S., Yamamoto, N., Fukuda, Y., 2011. A homogenization theory for elastic–viscoplastic ma-

terials with misaligned internal structures. International Journal of Plasticity 27, 2056–2067.

Meraghni, F., Chemisky, Y., Piotrowski, B., Echchorfi, R., Bourgeois, N., Patoor, E., 2014. Parameter identification of a thermodynamic model for superelastic shape memory alloys using analytical calculation of the sensitivity matrix. European Journal of Mechanics - A/Solids 45, 226–237.

Meraghni, F., Nouri, H., Bourgeois, N., Czarnota, C., Lory, P., 2011. Parameters identification of fatigue damage model for short glass fiber reinforced polyamide (PA6-GF30) using digital image correlation. Procedia Engineering 10, 2110–2116.

Mercier, S., Molinari, A., 2009. Homogenization of elastic-viscoplastic heterogeneous materials: Self-consistent and Mori-Tanaka schemes. International Journal of Plasticity 25, 1024–1048.

Michel, J. C., Suquet, P., 2004. Computational analysis of nonlinear composites structures using the nonuniform transformation field analysis. Computer Methods in Applied Mechanics and Engineering 193, 5477–5502.

Miled, B., Doghri, I., Brassart, L., Delannay, L., 2013. Micromechanical modeling of coupled viscoelastic-viscoplastic composites based on an incrementally affine formulation. International Journal of Solids and Structures 50, 1755–1769.

Mori, T., Tanaka, K., 1973. Average stress in matrix and average elastic energy of materials with misfitting inclusions. Acta Metallurgica 21 (5), 571–574.

Mura, T., 1987. Micromechanics of Defects in Solids. In: Mechanics of elastic and inelastic solids, Second, Revised Edition. Kluwer Academic Publishers, Dordrecht.

Paquet, D., Dondeti, P., Ghosh, S., 2011. Dual-stage nested homogenization for rate-dependent anisotropic elasto-plasticity model of dendritic cast aluminum alloys. International Journal of Plasticity 27, 1677–1701.

Pindera, M. J., Khatam, H., Drago, A. S., Bansal, Y., 2009. Micromechanics of spatially uniform heterogeneous media: A critical review and emerging approaches. Composites Part B: Engineering 40 (5), 349–378.

Praud, F., Chatzigeorgiou, G., Bikard, J., Meraghni, F., 2017. Phenomenological multi-mechanisms constitutive modelling for thermoplastic polymers, implicit implementation and experimental validation. Mechanics of Materials 114, 9–29.

Rao, W., Zhang, J., Kang, G., Yu, C., Jiang, H., 2019. A meso-mechanical constitutive model of bulk metallic glass composites considering the local failure of matrix. International Journal of Plasticity 115, 238–267.

Rémond, Y., 2005. Constitutive modelling of viscoelastic unloading of short glass fibre-reinforced polyethylene. Composite Science and Technology 65, 421–428.

Sadowski, P., Kowalczyk-Gajewska, K., Stupkiewicz, S., 2017. Response discontinuities in the solution of the incremental Mori-Tanaka scheme for elasto-plastic composites. Archives of Mechanics 69 (1), 3–27.

Simo, J. C., Hughes, T. J. R., 1998. Computational Inelasticity. Springer-Verlag, New York.

Wu, L., Adam, L., Doghri, I., Noels, L., 2017. An incremental-secant mean-field homogenization method with second statistical moments for elasto-visco-plastic composite materials. Mechanics of Materials 114, 180–200.

Wu, L., Noels, L., Adam, L., Doghri, I., 2013a. A combined incremental-secant mean-field homogenization scheme with per-phase residual strains for elasto-plastic composites. International Journal of Plasticity 51, 80–102.

Wu, L., Noels, L., Adam, L., Doghri, I., 2013b. An implicit-gradient-enhanced incremental-secant mean-field homogenization scheme for elasto-plastic composites with damage. International Journal of Solids and Structures 50, 3843–3860.

Zecevic, M., Knezevic, M., 2018. Latent hardening within the elasto-plastic self-consistent polycrystal homogenization to enable the prediction of anisotropy of AA6022-T4 sheets. International Journal of Plasticity 105, 141–163.

Highlights

1. A micromechanical model based on a modified multi-scale mean field approach combining Mori-Tanaka scheme combined with the Transformation Field Analysis is developed.

2. The modified mean field homogenization method considers a third phase as a coating between the fibers and the matrix in order to capture the distribution of local fields around the fiber observed in finite element based homogenization analyses.

3. This extension permits to address the overestimation of the global stress-strain response using the classical mean-field methods such as the Mori-Tanaka scheme without using isotropization techniques.

4. The new approach is applied to predict the overall behavior of long fiber reinforced elastoplastic and viscoelastic-viscoplastic composites under proportional and non-proportional multiaxial loading.